Physics – Uspekhi **54** (2) 119 – 144 (2011)

REVIEWS OF TOPICAL PROBLEMS

PACS numbers: **05.45. – a**, **45.50. – j**, **84.30. – r**

Dynamical chaos and uniformly hyperbolic attractors: from mathematics to physics

S P Kuznetsov

DOI: 10.3367/UFNe.0181.201102a.0121

Contents

Abstract. Research is reviewed on the identification and construction of physical systems with chaotic dynamics due to uniformly hyperbolic attractors (such as the Plykin attraction or the Smale–Williams solenoid). Basic concepts of the mathematics involved and approaches proposed in the literature for constructing systems with hyperbolic attractors are discussed. Topics covered include periodic pulse-driven models; dynamics models consisting of periodically repeated stages, each described by its own differential equations; the construction of systems of alternately excited coupled oscillators; the use of parametrically excited oscillations; and the introduction of delayed feedback. Some maps, differential equations, and simple mechanical and electronic systems exhibiting chaotic dynamics due to the presence of uniformly hyperbolic attractors are presented as examples.

S P Kuznetsov Saratov Branch, Kotel'nikov Institute of Radio-Engineering and Electronics, Russian Academy of Sciences
ul. Zelenaya 38, 410019 Saratov, Russian Federation
Tel. (7-8452) 27 86 85
E-mail: spkuz@rambler.ru

Received 1 April 2010, revised 16 September 2010
Uspekhi Fizicheskikh Nauk **181** (2) 121 – 149 (2011)
DOI: 10.3367/UFNr.0181.201102a.0121
Translated by S D Danilov; edited by A M Semikhatov

1. Introduction

One scientific area that has been rapidly developing in recent years is the study of complex dynamics and chaos in nonlinear systems [1–13].

An object of any physical nature is referred to as a dynamical system if its state at an arbitrary moment of time evolves from its initial state according to a certain rule established for this system. Notably, this definition does not exclude the possibility of chaotic behavior of the system, when the time dependence of observable quantities resembles a random process. The basic property of dynamical chaos is the exponential sensitivity to small perturbations, which makes it impossible to predict the state at times greater than a certain characteristic scale, which is logarithmically dependent on errors in the prescribed initial conditions ('the predictability horizon'). Chaos is encountered in systems of different natures, including mechanics, fluid dynamics, radio physics and electronics, laser physics and nonlinear optics, chemical kinetics, and biomedical objects.

In the state space of systems with dissipation, chaos is associated with the presence of a *strange attractor*. Approximately 40 years ago, a special kind of such attractors, called *uniformly hyperbolic*, was introduced in mathematical studies. They are encountered in systems that fall into the so-called *class of systems with axiom A* and make up a subject of the *hyperbolic theory* associated with the names Anosov, Alekseev, Smale, Williams, Sinai, Plykin, Ruelle, Pesin, Newhouse,

and others [14–25]. The chaotic nature of dynamics on uniformly hyperbolic attractors has been given a rigorous mathematical substantiation. Uniformly hyperbolic attractors demonstrate the property of structural stability: the structure of their phase space and characteristics of their dynamics are insensitive to variations of parameters and functions in the governing equations. At that time, it was expected that uniformly hyperbolic attractors would be pertinent to numerous physical situations related to chaos. But with the accumulation of concrete examples it has become apparent that they do not fit the narrow framework of the early hyperbolic theory. Therefore, uniformly hyperbolic attractors have been regarded as a purely academic representation of chaos, of no direct relevance to actual systems. The efforts of mathematicians have turned toward the development of generalizations that would be applicable to broader object classes. For example, the notions of quasihyperbolic, nonuniformly hyperbolic, and partly hyperbolic attractors and quasi-attractors were introduced [2, 19, 25–28].

The question of whether it is possible to propose physical systems whose dynamics would be governed just by the presence of a uniformly hyperbolic attractor appeared to have been abandoned for a long time and had remained unclarified until recently. In courses and reviews on nonlinear dynamics, such attractors are typically exemplified by models with a discrete time in the form of geometrical constructions explained on a qualitative level, for example, with the help of graphical images. Certainly, for a physicist, this is nothing more than a starting point. First and foremost, besides geometrical constructions, it is desirable to have examples based on explicitly written equations that would allow the use of computational techniques for analyzing dynamics and computing characteristics that are relevant for potential applications. Certain physical systems naturally admit a description in terms of discrete time, and it would be worthwhile to explore whether hyperbolic attractors are realized in them. Further, it is important to take a step toward continuous systems, because they are primarily interesting for physics and technology. It is desirable to formulate how the dynamics on a hyperbolic attractor can be implemented by combining structural elements known in the context of oscillation theory and its ramifications (oscillators, coupled systems, or feedback circuits). Finally, the models proposed in this way should be implemented as functioning devices, for example, in electronics, mechanics, or nonlinear optics, and their technological application should be drafted, together with substantiation of the advantages against possible alternative solutions.

Beginning from the classic work of Andronov and his school [29, 30], rough or structurally stable systems are considered to be of primary concern in the theory of oscillations and are regarded as very relevant from a practical standpoint. It seems that this same attitude should be expected to systems with structurally stable uniformly hyperbolic chaotic attractors. The absence of concrete physical examples is in obvious incongruity with this statement. From the methodological standpoint, the situation resembles that observed in the early 20th century with respect to limit cycles, before their role as a mathematical representation of auto-oscillations was established. In a similar vein, hyperbolic chaotic attractors should find their place as representation of phenomena in actual systems. This will, on the one hand, favor applications of the hyperbolic theory, developed by mathematicians, to the description of real-world phenomena, and on the other, complete the theory with physical relevance. This review aims at discussing the results obtained in this area.

2. Dynamical systems

The notion of a dynamical system is used if there is a set of variables, called *dynamical*, that fully determine the instantaneous state and a rule that enables predicting the system state at any subsequent moment of time if the initial state is given. The set of all possible states forms the *phase space*, whose dimension N is defined by the number of variables needed to specify a state. The time evolution of a state corresponds to motion of a point in this space along its *phase trajectory* or *orbit*. Systems with continuous time and systems with discrete time are considered. They are respectively referred to as *flows* and *cascades* in the mathematical literature.

The description of systems with continuous time relies on differential equations of the form $\mathrm{d}\mathbf{x}/\mathrm{d}t = \mathbf{f}(\mathbf{x})$, where $\mathbf{x}$ is an N-dimensional state vector and $\mathbf{f}$ is a vector function. By virtue of the existence and uniqueness theorem for solutions of differential equations, we can uniquely determine the states at subsequent, as well as preceding, instants of time given a system state at a certain instant of time. In other words, the state evolution can be followed both forward and backward in time.

If the function in the right-hand side of the differential equation explicitly depends on time, the system $\mathrm{d}\mathbf{x}/\mathrm{d}t = \mathbf{f}(\mathbf{x}, t)$ is called *nonautonomous*. In this case, to fully define the state, we need to specify, in addition to the vector $\mathbf{x}$, the instant of time to which the vector $\mathbf{x}$ is related. Therefore, the augmented space with dimension $N + 1$ is introduced, which is referred to as the *augmented phase space* in this context. In this review, when addressing nonautonomous systems, we assume only a periodic dependence of functions $\mathbf{f}$ on time.

Systems with discrete time are defined with the help of a map that describes the transformation of a state in a single time step, $\mathbf{x}_{n+1} = \mathbf{g}(\mathbf{x}_n)$, where $\mathbf{x}$ is the state vector and $\mathbf{g}$ is a vector function. The phase trajectory then reduces to a discrete sequence of points.

Both system classes, with continuous and discrete time, are closely related. The transition from the former to the latter is enabled through the construction known as the *Poincaré section*. A section of the phase space of a system with continuous time is selected such that phase trajectories repeatedly intersect it.[1] In this case, a function can be introduced that establishes a correspondence between an arbitrary point in the section and the point at which the trajectory passing through the original point intersects the section surface once again. This function defines the *Poincaré map*. If the coefficients of differential equations are smooth functions of dynamical variables, then the map represents a *diffeomorphism*, i.e., is defined by a continuously differentiable function having a uniquely defined inverse function, which is also continuously differentiable.

For a nonautonomous system whose right-hand side varies with a time period T in the respective differential equation, the standard way of constructing the Poincaré map is to consider the system dynamics stroboscopically, following its states $\mathbf{x}_n$ at time instants $t = t_0 + nT$. This corresponds to taking sections of the augmented phase

[1] More precisely, a hypersurface of codimension one is understood here.

space by the family of planes $t = t_0 + nT$ and defining the map from one plane to the next one, with the number incremented by one.

The reconstruction of a system with continuous time from a given invertible map is called the suspension.[2]

In order to distinguish between regular and chaotic dynamics on a quantitative level, the *Lyapunov exponents* are used. We assume that there is a trajectory staying in a finite domain of phase space and a neighboring trajectory slightly differing from the first one due to a small difference in its initial conditions. As long as the perturbation remains small, the time evolution of the state difference vector is described (up to an unimportant amplitude factor) by the relation $\tilde{\mathbf{x}} \sim \exp(\lambda_i t)$, where λ_i is a Lyapunov exponent. Each trajectory has a set of N exponents λ_i, $i = 1, \ldots, N$ (the phase space dimension), which is called *the Lyapunov exponent spectrum*. A positive exponent implies that a neighboring trajectory is moving away from the given orbit, and a negative one implies that the trajectories are approaching each other.

The procedure of numerically computing Lyapunov exponents [6, 11, 31] consists in solving the system of equations $\mathrm{d}\mathbf{x}/\mathrm{d}t = \mathbf{f}(\mathbf{x})$ that define the motion along a given trajectory together with N sets of equations, linearized with respect to this trajectory, for the perturbation vectors, $\mathrm{d}\tilde{\mathbf{x}}/\mathrm{d}t = \mathbf{f}'(\mathbf{x})\,\tilde{\mathbf{x}}$, where $\mathbf{f}'(\mathbf{x})$ is the matrix derivative of a vector function. For systems with discrete time, accordingly, iterations of the map $\mathbf{x}_{n+1} = \mathbf{g}(\mathbf{x}_n)$ are taken together with iterations of the linearized maps $\tilde{\mathbf{x}}_{n+1} = \mathbf{g}'(\mathbf{x}_n)\,\tilde{\mathbf{x}}_n$. In the process of computation, the vectors $\tilde{\mathbf{x}}$ are made orthogonal by the Gram–Schmidt procedure and are normalized to a fixed norm. The Lyapunov exponents are obtained as slopes of the lines that approximate the accumulated sums of logarithms of ratios of vector norms before and after normalization.

There is a distinction between *conservative* and *dissipative* systems. Conservative systems are characterized by their ability to keep a 'memory' of their initial state. For example, oscillations of a pendulum preserve the amplitude set by the initial perturbation in the absence of friction. In contrast, 'memory loss' is inherent in dissipative systems, such that in a system evolving on its own over a long time interval, the regime of dynamics becomes independent of the initial state. Examples are provided by a pendulum in the presence of friction or an electronic generator of periodic auto-oscillations.

An attractor in the phase space of a dissipative system is an object that corresponds to a sustained regime of dynamics. The simplest example of an attractor is provided by a stable equilibrium state. Another simple example is a stable limit cycle, a closed phase trajectory that serves as a mathematical representation of periodic auto-oscillations.

The spectrum of Lyapunov exponents is understood as the spectrum of a typical trajectory on the attractor. The presence of at least one positive Lyapunov exponent in the spectrum signals that the attractor is chaotic. The sum of all N exponents must be negative. For autonomous systems with continuous time, an attractor different from an attracting fixed point must have a zero Lyapunov exponent in its spectrum, which is associated with a perturbation representing a shift along the phase trajectory.

Strange attractors exhibit a fractal structure. If the spectrum of Lyapunov exponents is known, the attractor fractal dimension can be estimated by the Kaplan–Yorke formula [6, 11, 32]

$$D = m + \frac{\sum_{i=1}^{m} \lambda_i}{|\lambda_{m+1}|},$$

where the number m is determined from conditions $S_m = \sum_{i=1}^{m} \lambda_i > 0$, $S_{m+1} < 0$.

3. Interpretation of dynamics in terms of phase fluid and simple examples of hyperbolic attractors

We consider an ensemble composed of a large number of similar noninteracting dynamical systems that differ only by their initial conditions. In the phase space, this ensemble is represented by a cloud of points, which changes its size and shape as the points move according to the dynamical equations of the individual system. In dissipative systems, the volume of the cloud decreases and eventually 'condenses' on an attractor (or, possibly, several attractors).

Chaotic dynamics occur when the cloud of representing points undergoes repeated transformations of dilation, folding, and contraction. As an illustration, we consider a dissipative version of the so-called *baker map* [6, 11] (Fig. 1). We take a unit square on the plane (x, y) and deform it such as a baker rolls pastry, assuming that its horizontal size increases twofold and its vertical size reduces threefold. The total area decreases, which manifests the dissipative nature of the map; the 'pastry' in this case should be conceived of as a compressible substance. Next, we cut the pastry into two halves and place the halves one above the other, aligning them with the top and bottom sides of the unit square and leaving a gap between them. After multiple repetitions, we obtain a system of horizontal strips, their number increasing as 2^n (n is the number of iterations), and their total width decreasing proportionally to $(2/3)^n$. Notably, the dynamics of an individual pastry particle is chaotic.[3] The attractor represents an object occurring in the limit of infinitely many iterations. It has the structure of a *Cantor set* in its transverse

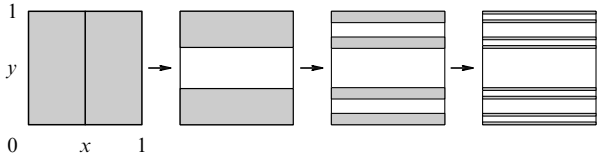

Figure 1. Geometric illustration of the action of a dissipative baker map.

[2] The suspension is usually understood as a flow system for which the required map is realized over a time that is independent of the initial state. This is associated with constructing a system of differential equations with coefficients that are periodic in time. In the more general case of a system for which the map of a given form represents the Poincaré map, the term *special flow* is used.

[3] For an individual 'pastry' particle, the evolution of coordinates (x, y) with respect to the discrete time n is described by the equations $x_{n+1} = 2x_n$ and $y_{n+1} = 1/3y_n$ for $x_n \leqslant 1/2$ and $x_{n+1} = 2x_n - 1$ and $y_{n+1} = 1/3y_n + 2/3$ for $x_n > 1/2$. To deduce that its dynamic is chaotic, we represent the initial value of x as a number in binary notation, for instance, as 0.0110010110111... One step of evolution implies a shift in this sequence one position to the left, discarding the leftmost digit. The digit 0 or 1 in the first position after the binary point shows whether the particle is in the left or right half of the unit square at this instant of time. For an initial condition taken arbitrarily, we obtain an arbitrary sequence of zeros and ones in binary notation such that the representing point goes into the left and right halves of the square in a random sequence.

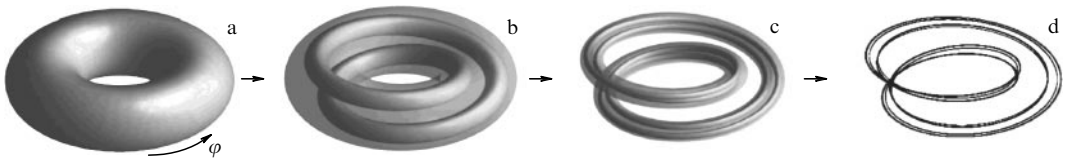

Figure 2. An absorbing torus-shaped domain in a three-dimensional phase space (a), the result of its transformation after two iterations (b, c), and the Smale–Williams solenoid appearing after multiple map iterations (d).

sections. We note that the pastry density is distributed along the strips uniformly.

Despite its simplicity, the baker map illustrates many intrinsic features of chaotic attractors, for example, the presence of a transverse Cantor structure and the combination of stability, in the sense that the representing points approach the attractor, and instability, in the sense that they scatter along the fibers of the attractor.

Cutting the pastry in this construction is admittedly dissatisfying. We may try to avoid it, assuming that after being rolled out, the pastry is not cut but folded such that it fits the unit square once again. In this case, at the first steps of the iterations, we can also see the formation of a layered structure. But in the limit of a large number of iterations, we do not obtain a uniform distribution along the fibers, nor even a distribution approaching the uniform one! The substance has a tendency to accumulate at fold locations, forming singularities in its density distribution. The cause stems from the fact that in the vicinity of bends, the direction of contraction coincides with the vertical tangent at the boundary of the pastry piece and a domain of increased density emerges as it is rolled out. In a nonlinear dissipative system, this might eventually be associated with nonhyperbolic chaos or the condensation of the cloud on regular attractors (fixed points and cycles).

The hyperbolic chaos corresponds to a situation where the transformation of a cloud of representing points in phase space, comprising longitudinal dilation and transverse contraction, is carried out uniformly, without discontinuities or localized regions of increased density.

That the attractors with such properties are possible follows from considering a number of appropriate, elaborately constructed examples. In the process of construction, a domain in the phase space called *absorbing* is identified, together with the evolution rule in a discrete time, such that this domain be mapped into itself in one map iteration. The attractor is then obviously located inside the absorbing domain.

The first example is the *Smale–Williams attractor* [1–24], which is given by a map in three-dimensional space. We consider a torus-shaped domain. Regarding it as an elastic doughnut-shaped roll, we stretch it along its length and compress it in the transverse direction, fold it to form a double loop, and put it inside the original torus (Fig. 2). To ensure that the construction just obtained fits there, we have to assume that the transverse direction is compressed more than twofold. At each iteration, the total volume is reduced (dissipation), while the number of loops is doubled. In the limit, as the number of loops tends to infinity, the so-called *solenoid* emerges with a Cantor structure in its transverse section.[4] An essential point here is that the angular coordinate

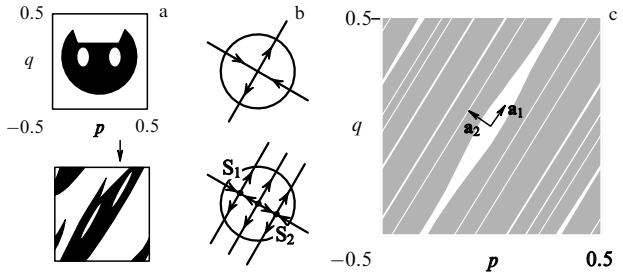

Figure 3. (a) Illustration of the action of the Anosov hyperbolic map, also called the Arnold cat map, on points of a unit square that represents an unrolled torus. (b) Schematics explaining the modification of the map in the neighborhood of a fixed point, which makes up the essence of Smale surgery, needed to pass to the map with a DA attractor. (c) The portrait of the attractor in a unit square.

φ is doubled (see Fig. 2). A generalization of this construction is achieved by folding such that a loop with M turns is formed, which corresponds to the map $\varphi_{n+1} = M\varphi_n \pmod{2\pi}$ for the angular coordinate. For $M \geqslant 2$, this map is referred to as *the dilating circle map* or *the Bernoulli map*.

The *DA attractor* (Derived from Anosov) proposed by Smale is defined through a two-dimensional map on the surface of a torus [14, 17, 19, 20]. The starting point is the Anosov map $p_{n+1} = p_n + q_n$ and $q_{n+1} = p_n + 2q_n \pmod 1$, where $\varphi = 2\pi p$ and $\theta = 2\pi q$ are angular coordinates on the torus. The phase space can be conveniently represented by unrolling the torus into a unit square (Fig. 3). The Anosov map is conservative and has a saddle-type fixed point at the origin, with stable and unstable directions determined by the vectors $\mathbf{a}_1 = (1, W)$ and $\mathbf{a}_2 = (-W, 1)$, where $W = (\sqrt{5}+1)/2$.

To ensure the presence of an attractor, it is suggested to modify the map and make it dissipative through surgery in a small neighborhood of the fixed point. The modification is performed such that the motion along the unstable direction undergoes no changes, but the fixed point becomes repelling along the orthogonal direction, such that saddle points $\mathbf{S}_1$ and $\mathbf{S}_2$ form in its proximity (Fig. 3b). Outside the region subject to surgery, the map preserves its form.

The absorbing domain is the whole torus surface except the cut-out vicinity of the origin. As a consequence of iterations, the cut-out part is stretched parallel to the vector $\mathbf{a}_1$ and simultaneously contracted along the orthogonal direction $\mathbf{a}_2$ such that sprouts turn into narrow strips aligned with the unstable direction. Because the slope is given by an irrational number, these strips cover the torus densely (Fig. 3c). In this way, a transverse Cantor structure characteristic of a hyperbolic attractor is formed. A particu-

[4] The solenoid as a mathematical object was introduced by mathematicians Vietoris and van Dantzig [19]. It appears as a chaotic attractor in studies by Smale [14] and Williams [15]. Interestingly, the solenoid is met in the theory of dynamical systems in yet one more context, as a nonchaotic attractor at a critical point where bifurcations of period doubling according to Feigenbaum [33] accumulate. (In this last case, the formation of each new level of fractal structure is associated with doubling the time scale, and not with the iterative step, as it is for the Smale–Williams attractor.)

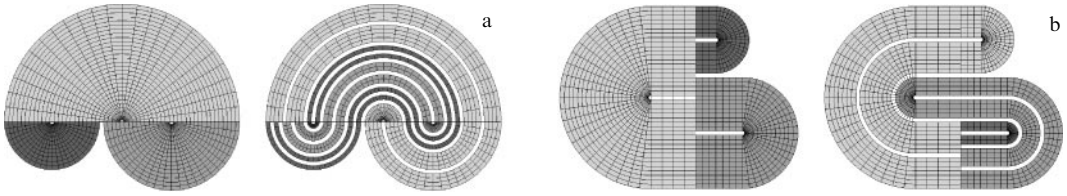

Figure 4. The absorbing domain of an attractor and the result of its transformation under the map for two variants (a and b) of the Plykin attractor.

lar variant of such an attractor is described in Ref. [34], dedicated to computer illustrations of the hyperbolic theory objects.

A Plykin attractor [17, 19, 20, 35] occurs in a special two-dimensional map on a plane. Figure 4a shows a domain composed of three semidisks with small semicircular cuts. It is hatched by lines showing two fields of directions prescribed in this domain. We define the map so as to arrive at the picture in the right panel of Fig. 4a as a result of the map action on the points of the given domain. The fields of directions coincide with the original ones upon applying the map, dilation occurs along one of them, and contraction occurs along the other one. This ensures the hyperbolic nature of the attractor.

Currently, it is known that in a finite planar domain with three or more holes, many hyperbolic attractors can be constructed differing in design [15, 36, 37]. They are referred to as *Plykin-type attractors*. One of the modifications, of special interest for the subsequent presentation, is illustrated in Fig. 4b. Plykin-type attractors can also be considered on a sphere. Mapping from the plane to the sphere or back corresponds to a transformation of variables given by the stereographic projection, which is known from elementary geometry. The minimum number of holes needed on a sphere for enabling a uniformly hyperbolic attractor is four.[5]

4. Basic concepts of the hyperbolic theory

It is appropriate to begin an introduction to the hyperbolic theory by discussing a fixed saddle-type point. Figure 5a shows a pendulum and its phase portrait on the plane $(\varphi, \dot{\varphi})$, where φ is the angle from the vertical and $\dot{\varphi}$ is the instantaneous angular velocity. The pendulum may oscillate around its lower equilibrium position $\varphi = 0$, but we are currently interested in the unstable equilibrium, $\varphi = \pi$. In the phase space, it corresponds to saddle point A located at the intersection of curves called separatrices. Under a small perturbation, the representing point leaves the equilibrium position along the unstable separatrix U. On the other hand, let a precisely computed momentum be imparted to the pendulum in its lower equilibrium position such that the pendulum reaches the upper equilibrium and comes to rest there. In this case, the representing point follows the curve S called a stable separatrix. The saddle point regarded as a phase trajectory is hyperbolic. (The terminology derives from the fact that the phase trajectories in a local neighborhood of the saddle look like hyperbolas.)

A general saddle trajectory with similar properties can be considered (Fig. 5b).

[5] This agrees with the previous statement. Indeed, if the center of the projection (mapped to infinity by the stereographic projection) is placed inside one of the holes on the sphere, then we obtain an attractor localized in a finite domain with just three holes in the planar geometry.

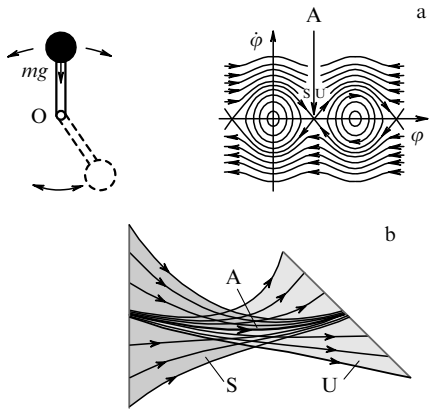

Figure 5. The concept of a saddle hyperbolic trajectory. (a) A pendulum and its phase portrait containing the fixed saddle-type point A. (b) The structure of phase space in the vicinity of the general type of a saddle trajectory. Letters S and U respectively label the stable and unstable manifolds.

A trajectory is called *hyperbolic* if at each of its points, two subspaced can be defined in the vector space of all possible infinitesimally small perturbations (the tangent space): a subspace of vectors V_S such that their norm exponentially decreases as they evolve forward in time and a subspace of vectors V_U whose norm exponentially decreases backward in time. In flow systems, for trajectories distinct from fixed points, there is, additionally, a neutral subspace that corresponds to perturbations along a trajectory that neither increase nor decrease on average. An arbitrary vector of a small perturbation must admit a decomposition into a linear combination of vectors belonging to the above subspaces.

A set of points that approach a given trajectory in the course of evolution is called the *stable manifold* of this trajectory. Similarly, the *unstable manifold* is the set of points approaching the given trajectory for the evolution backward in time. For hyperbolic orbits, these are true manifolds, i.e., smooth curves, surfaces, or hypersurfaces, which is a statement of a special theorem.

Hyperbolic saddle trajectories can occur in the phase space for both conservative and dissipative systems, but in this review, we consider only the dissipative case.

A uniformly hyperbolic chaotic attractor is an attracting object in the phase space of a dissipative system composed exclusively of saddle trajectories, such that the phase space has a similar structure in local neighborhoods of all these trajectories. For all trajectories on the attractor, the manifolds must have the same dimension. Intersections between the stable and unstable manifolds are allowed only at finite angles (tangential contact is forbidden).

For the Smale–Williams attractor, the stable manifolds correspond to the family of meridional sections of a torus with planes $\varphi = \text{const}$ (see Fig. 2). The unstable manifold for any point on the attractor represents a fiber of a solenoid

passing through this point, while taken as a whole it coincides with the attractor proper. For a DA attractor, the stable manifolds are one dimensional, as are the unstable ones. The unstable manifolds are stretched along a vector $\mathbf{a}_1$, while the stable ones are stretched along a vector $\mathbf{a}_2$ orthogonal to $\mathbf{a}_1$. For a Plykin-type attractor, the stable manifolds are associated with families of lines along which the phase volume is contracted (see Fig. 4). The unstable manifolds extend along the second family of lines that corresponds to directions of dilation.

5. The contents and conclusions of the hyperbolic theory

We turn to a brief survey of the hyperbolic theory [14–24]. For simplicity, we consider systems with discrete time (maps). The results can be extended to systems with continuous time by passing to the description in terms of the Poincaré maps.

We begin by discussing *axiom A*, a proposition formulated by Smale, which (augmented by the requirement of strict transversality) allows segregating a class of structurally stable systems among dynamical systems of an arbitrary finite dimension.

A point in the phase space of a dynamical system is called *wandering* if it has a neighborhood such that a trajectory emanating from this point never returns to that neighborhood after a certain instant of time. From a physical standpoint, such dynamics correspond to transient processes. All other points are classified as *nonwandering*. Axiom A for a system with discrete time, defined in terms of a diffeomorphism $\mathbf{g}$, assumes, first, that the set of nonwandering points NW is hyperbolic and, second, that the periodic points of the map $\mathbf{g}$ form a dense subset in NW. The last statement means that in an arbitrarily small neighborhood of the set NW, there necessarily exists a point of some periodic orbit that belongs to the same set.[6] The hyperbolicity is understood as explained above: we assume that the linear space of perturbation vectors is composed of subspaces V_U and V_S corresponding to exponential dilation and contraction of vectors as they evolve with time.[7] The condition of strict transversality requires that the positions of stable and unstable manifolds relative to each other be structurally stable for an arbitrary pair of points belonging to the set NW, i.e., only intersections at a finite angle are allowed (tangential contacts are forbidden).

For systems with axiom A, a theorem on spectral decomposition, proved by Smale [2, 14], is valid. It states that the set of nonwandering points can be represented as a union of finitely many nonintersecting invariant sets B_i having the transitivity property (i.e., each such set includes a trajectory that visits an arbitrarily small vicinity of any point in the set), which are called *basic* or *locally maximum sets*. For various particular systems, such sets may be stable or unstable fixed points, periodic orbits, or nontrivial attracting, repelling, or saddle invariant sets. The definition of a locally maximum set assumes that it is represented as an intersection of images of a certain neighborhood containing it, obtained by iterating the map forward and backward in time. This can be likened to the definition of an attractor as the intersection of images of an absorbing domain in iterations in direct time, and such an attractor may emerge as a particular case of the basic set. Further, each basis set can be represented as a union of a finite number $k_i \geqslant 1$ of nonintersecting subsets $X_{i,y}$ visited sequentially in a certain order in map iterations. Each set $X_{i,y}$ is the invariant set for the map applied k_i times.

Uniformly hyperbolic Plykin and Smale–Williams attractors or the DA attractor are basic sets of model dynamical systems with axiom A for which $k = 1$ (i.e., they cannot be further decomposed into components). In this review, we restrict ourself to attractors of this kind and do not consider the case $k > 1$. Moreover, unless specially mentioned, only attractors with one-dimensional unstable manifolds are considered.

A criterion of hyperbolicity exists that has been proved on the level of a mathematical theorem — the *cone criterion* [16, 17, 20, 22, 23], which can be tested in numerical simulations.

Let the dynamics in discrete time be defined by a smooth map $\bar{\mathbf{x}} = \mathbf{f}(\mathbf{x})$. The cone criterion requires that for some choice of a constant $\gamma > 1$ for each point $\mathbf{x}$ on the trajectory in the space of vectors of infinitesimal perturbations (tangent space), the expanding and contracting cones can be defined (Fig. 6). The expanding cone is the set of infinitesimal perturbation vectors whose norm increases by a factor $\gamma > 1$ or greater as a result of applying the map $\bar{\mathbf{x}} = \mathbf{f}(\mathbf{x})$. The contracting cone is the set of vectors whose norm increases by a factor γ or greater under the action of the inverse map $\tilde{\mathbf{x}} = \mathbf{f}^{-1}(\mathbf{x})$. Bearing in mind the smooth dependence of all objects considered here on the position of a point in the phase space, we can speak about fields of expanding and contracting cones. These cones should be invariant in the sense that for every point $\mathbf{x}$ on a given trajectory, the image of the expanding cone must be inside the expanding cone defined for the image point, and the pre-image of the contracting cone must be inside the contracting cone defined for the pre-image point.

What consequences can be deduced from the hyperbolic nature of an attractor?

Instability. The fact that an attractor is composed of unstable manifolds implies that the motion on the attractor is sensitive to small initial perturbations, which is the main attribute of dynamical chaos. Indeed, two representing points, being slightly displaced relative to each other along the unstable manifold, move apart as time progresses. As long as the perturbation remains small, it increases on average according to an exponential law, $||\Delta\mathbf{x}|| \sim \exp(\Lambda n)$, where n is the discrete time and $\Lambda > 0$ is the largest Lyapunov exponent.

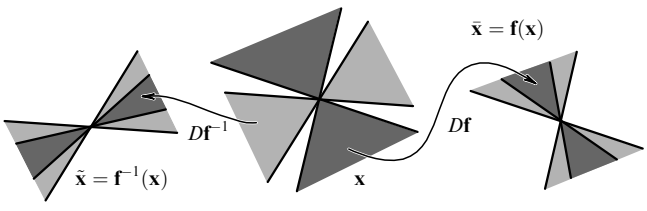

Figure 6. Clarification of the hyperbolicity criterion. For a point $\mathbf{x}$, the image of the expanding cone is located inside the expanding cone defined for the image point $\bar{\mathbf{x}} = \mathbf{f}(\mathbf{x})$, while the pre-image of the contracting cone is located inside the contracting cone for the pre-image point $\tilde{\mathbf{x}} = \mathbf{f}^{-1}(\mathbf{x})$. $D\mathbf{f}$ and $D\mathbf{f}^{-1}$ are matrix derivatives of the direct and inverse maps that define the transformation of perturbation vectors in one forward or backward step.

[6] One particular subclass of systems with axiom A is exemplified by Anosov systems, such as the Arnold cat map, whose specificity is that their sets of nonwandering points occupy the whole phase space.

[7] Situations when one of the subspaces, V_U or V_S, is an empty set are not excluded, which, in particular, allows structurally stable systems with simple nonwandering sets like fixed points or periodic orbits to be included in the framework of the picture based on axiom A.

If unstable manifolds are one-dimensional, the spectrum of Lyapunov exponents contains a single positive value, with the others being negative. We stress that for the maps, all Lyapunov exponents of a uniformly hyperbolic attractor are separated from zero. Indeed, for individual trajectories on an attractor, the perturbation vectors belonging to expanding cones defined at points of these trajectories correspond to positive exponents. Because the degree of expansion is bounded from below by a constant $\gamma > 1$, the positive Lyapunov exponent cannot be smaller than $\Lambda^{+}_{\min} = \ln\gamma$. This is true for all trajectories that belong to the attractor, and hence the estimate is also valid for an exponent that pertains to the attractor as a whole. Analogously, negative Lyapunov exponents associated with vectors that belong to contracting cones are bounded from above by the constant $\Lambda^{-}_{\max} = -\ln\gamma$.

Markov partitions and symbolic dynamics. Because a structure formed by stable and unstable manifolds is present in the neighborhood of an attractor, the domain comprising the attractor can be partitioned into a finite number of nonintersecting single-connected subdomains whose boundaries follow along lines or surfaces that correspond to these manifolds. If certain conditions are satisfied [2, 16, 17, 10, 13, 24] (in particular, the images of boundary segments that go over stable manifolds must reappear at boundaries of the same type under the action of the map), this partition, called the *Markov* partition, can be used as a basis of the complete description of the motion on an attractor in terms of *symbolic dynamics*.

Denoting each element of the partition by a certain symbol (a letter), we encode a trajectory as a sequence of these symbols in the order the respective domains are visited. For specific attractors, these sequences can be subjected to certain limitations — 'grammar rules' — that can be explicitly represented in terms of a graph with a finite number of vertices and directed edges. Associated with the graph is its *adjacency matrix*, whose elements are 0s and 1s, with the (i, j) entry equal to 1 if an edge goes from node i to node j and 0 otherwise. Figure 7 illustrates Markov partitions and graphs for the Smale–Williams attractor and a Plykin-type attractor. These graphs apparently indicate that a transition from each vertex to any other vertex is possible in a finite number of steps along the directed edges. In addition, more than one edge emerges from some of the vertices.[8] This implies that in the process of constructing a symbolic sequence, the transition from such a vertex can be chosen at random from the existing alternatives. Any code obtained in this manner necessarily corresponds to a trajectory on the attractor for some choice of the initial conditions. The trajectory demonstrates chaotic behavior, visiting the partition domains as dictated by the given random sequence. The behavior can be interpreted as a Markov chain [38] — a random process with discrete time and a finite discrete set of states associated with symbols of an alphabet or elements of a partition (which is the origin of the term 'Markov partition').

The set of trajectories belonging to a hyperbolic attractor is in a one-to-one correspondence with the set of infinite sequences composed of letters of a finite alphabet that respect the grammar rules. It has the power of the continuum. The set

[8] In this case, the adjacency matrix has the transitivity property (which means that being raised to some sufficiently high power, it gives a matrix all of whose entries are nonzero) and the attractor, as stated, has a unique transitive component.

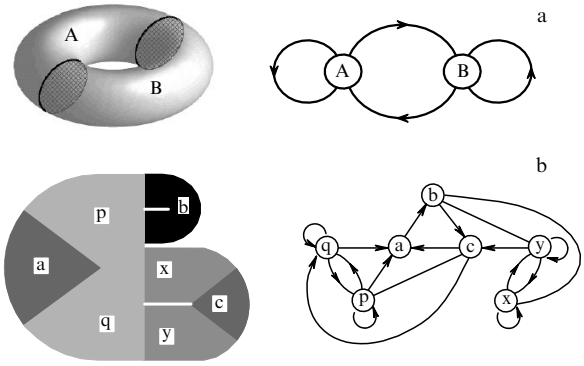

Figure 7. The Markov partition and pictures of graphs that define allowed transitions for Smale–Williams (a) and Plykin (b) attractors.

of periodic orbits on an attractor corresponds to periodic symbolic consequences and has the power of a countable set. As the period of periodic orbits P increases, their number N_p increases exponentially as $N_P \sim \exp(h_T P)$, where $h_T > 0$ is called the *topological entropy* [39, 40]. It is interpreted as a complexity measure for the set of trajectories of a dynamical system.

Clearly, the possibility of providing the full symbolic description of trajectories on a uniformly hyperbolic attractor allows treating dynamical process in the context of ideas inherited from information theory and coding. This may be important from the standpoint of using systems with such attractors in applications involving information processing and communications.

Structural stability [2, 14–23] of a uniformly hyperbolic attractor is inferred from the fact that dilation and contraction in the phase space always occur along directions that form a nonzero angle. In terms of stable and unstable manifolds, this corresponds to their transversal (not tangent) mutual position at intersection. If the parameters or functions involved in the definition of dynamical systems are varied (which is sometimes expressed as 'wiggling the system'), then, owing to the transversal intersections of the manifolds, the topology of the space partition does not change up to this point, as long as wiggling is not excessively strong. This is related, among other things, to the system of lines and surfaces used in constructing the Markov partition; hence, the symbolic dynamics are preserved without changes.

A more precise formulation is as follows: as long as weak wiggling is considered in the class of functions continuous together with their first derivatives (functions of the C^1 class according to the accepted terminology), the system admits a transformation to the original state via changes of variables that are one-to-one and continuous in both directions, i.e., the system remains topologically equivalent to the original system.

Lyapunov exponents are determined from the equations in variations obtained as a linearization of the original equations near a trajectory that belongs to the attractor. The procedure involves the application of the differentiation operation. As a result, the Lyapunov exponents are generally not invariant under the change of variables, which is typically not smooth. Nevertheless, because of structural stability, certain conclusions can be drawn concerning their behavior under small wiggling. As long as the attractor remains uniformly hyperbolic and preserves its structure of stable and unstable manifolds, the numbers of positive and negative exponents cannot change. Moreover, they both certainly

remain bounded from zero. Arguably, even a stronger conjecture is valid: for small wiggling of the system, the variation of at least the positive Lyapunov exponent is also small. This finds support in the numerical data for models with uniformly hyperbolic attractors discussed in Sections 7–9. But the author is unaware of rigorous mathematical results that can be referred to in this context.

Due to structural stability, trajectories on a uniformly hyperbolic attractor exhibit the property of *shadowing*, which is manifested in the fact that if an arbitrary weak perturbation (including a time-dependent one) is applied to the system, for any phase trajectory of the system, a trajectory of the original unperturbed system can be selected such that the two trajectories stay close to each other during their entire evolution in time. This pertains, in particular, to systems affected by noise of a limited intensity. This remarkable result, obtained in due time by Kifer [41], bears witness that the dynamic stochasticity dominates, in a certain sense, over the stochasticity related to small random external perturbations.

Existence of an absolutely continuous invariant measure of Sinai–Ruelle–Bowen [2, 42–44]. We return to the interpretation of dynamics as the evolution of a cloud of representing points in phase space. Supposing that at the initial instant of time the ensemble is characterized by a 'good' distribution function (continuous and decaying sufficiently fast toward the ends), we ask the question: What is the character of the distribution as time progresses? It can be easily verified that even in the simplest situations, the distributions emerging in the limit $t \to \infty$ can be singular, like, for example, Dirac's delta function in the case of a stable equilibrium state. A generalization that embraces both smooth and nonsmooth distributions can be obtained by invoking the mathematical concept of measure. Specifying a measure means establishing a correspondence between a subset of the phase space (not arbitrary but belonging to a sufficiently broad class of measurable sets) and some nonnegative number, additionally demanding that certain conditions be satisfied (for example, that a disjoint union of measurable sets have the measure equal to the sum of the measures of the parts).

We consider a phase trajectory on an attractor and make an agreement that the measure associated with any domain is equal to the relative fraction of time the representing point spends there in the limit of infinite observation time. For uniformly hyperbolic attractors, the measure constructed in this manner turns out to be the same for typical trajectories; it is the so-called *Sinai–Ruelle–Bowen measure*. It is associated with the distribution of phase fluid along the attractor fibers, i.e., on unstable manifolds, such that the substance is distributed smoothly along the fibers, ensuring that the distribution density is free of local singularities. The term *absolutely continuous invariant measure* is used in the mathematical literature.

Motion on a uniformly hyperbolic attractor has the properties of *ergodicity* and *mixing* [2, 16–23].[9] The ergodicity means that as it evolves in time, a typical trajectory on the attractor visits any neighborhood of an arbitrary point on the attractor. This implies the equivalence of time averaging and averaging over the invariant measure and allows applying a statistical approach to the analysis of stationary dynamical regimes. The mixing property, which is stronger, is manifested in the fact that the cloud of representing points corresponding to some element of the phase space spreads with time over the whole attractor after a sufficiently long time. In the framework of the statistical method, the mixing property allows describing the approach of an ensemble of systems to the state that corresponds to a stationary invariant distribution. The mixing property is also associated with the decay of correlations: the correlation function computed for a signal spawned by dynamics on a uniformly hyperbolic attractor in a system with discrete time decays exponentially. (For systems corresponding to the suspension of diffeomorphisms with uniformly hyperbolic attractors, the question about mixing and correlation decay in continuous time requires special analysis in each particular case because it depends on the character of the distribution of return times into the Poincaré section.)

Metric entropy of Kolmogorov and Sinai [45, 46]. We consider all possible n-symbol 'words' encountered in the symbolic coding of trajectories on an attractor and for each of them determine the probability of their occurrence p_i. The probability p_i can be interpreted as the Sinai–Ruelle–Bowen measure for the set of points in the phase space related to trajectories that at the preceding n steps visited the elements of the Markov partition denoted by the respective symbols. We determine the sum $S_n = \sum p_i \log p_i$ over all words allowed by the grammar, divide it by n, and take the limit as $n \to \infty$. The quantity $h_{\mathrm{KS}} = -\lim_{n\to\infty} S_n/n$ is called the *metric entropy* or the *Kolmogorov–Sinai entropy*. As can be seen from its definition, the metric entropy can be interpreted as the amount of information generated by the dynamics on the attractor per unit time. Notably, the definition invokes an invariant measure defined on the attractor. The positivity of h_{KS} serves as a criterion of the chaotic nature of the attractor. The entropy h_{KS} is related to the topological entropy by the inequality $h_{\mathrm{T}} \geqslant h_{\mathrm{KS}}$. The result proved in [47] establishes a relation between the Kolmogorov–Sinai entropy and the spectrum of Lyapunov exponents: The Kolmogorov–Sinai entropy is equal to the sum of positive Lyapunov exponents $h_{\mathrm{KS}} = \sum_{\Lambda_i>0} \Lambda_i$.

6. Work related to the search for uniformly hyperbolic attractors

At the beginning of the 1970s, Ruelle and Takens proposed a concept according to which the transition to chaos governed by a parameter, such as the Reynolds number in fluid dynamics, proceeds through the excitation of a small number of oscillatory motion components and that this transition stems from the appearance of a strange attractor [48]. In the context of this review, we emphasize that the authors of Ref. [48] meant not just a strange attractor in the broad sense of this word, as used currently, but precisely a uniformly hyperbolic attractor. The mathematical theorem underlying the concept is formulated in application to three situations [49]: for diffeomorphisms on (1) a two-dimensional compact manifold, (2) a two-dimensional torus, and (3) a compact manifold of dimension $m \geqslant 3$. In case 1, it is proved that a map having a hyperbolic attractor can be found arbitrarily close to the identity map in the class C^1 (of functions with the first derivative). In case 2, an analogous statement is true, but in the sense of closeness in the class C^2 (of functions with two derivatives), and in case 3, in the class of infinitely differentiable functions C^∞.

As follows from the analysis of the proof, constructions 1 and 2 bear an absolutely unphysical character because

[9] To simplify formulations, the attractors containing a single transitive component are meant.

defining the map involves functions of a complex structure at small scales in the phase space. The authors rely on the existence of a two-dimensional map with a hyperbolic attractor as a known fact when conducting the proof in all three cases; therefore, this approach can hardly be helpful in searching for particular examples.

One of the most famous systems in the context of complex dynamics and chaos is the Lorentz model [50], which is described by the system of equations $\dot{x}=\sigma(y-x)$, $\dot{y}=rx-y-xz$, $\dot{z}=-bz+xy$, where σ, r, and b are parameters (the classical Lorentz attractor is realized for $\sigma=10$, $r=28$, and $b=8/3$). An essential step in explaining the qualitative side of chaotic dynamics is the construction of a simplified model, the so-called geometric Lorentz attractor [21]. The computer proof by Tucker [51] of the chaotic nature of the Lorentz attractor with the help of a rigorously substantiated computer procedure serves as a sort of concluding research result.

The Lorentz attractor is identified as a *quasihyperbolic* or *singular hyperbolic* because it includes a special trajectory (an unstable manifold of a fixed point located at the origin). Therefore, the Lorentz attractor does not exhibit structural stability in its common sense, and although its Markov partition can be constructed, this cannot be done with a finite alphabet. The question of whether the system can be modified such that the attractor becomes uniformly hyperbolic is answered positively in [52], but only on the level of geometrical construction. The model considered is similar to the geometric model of the Lorentz attractor, in which a fixed point experiences a bifurcation that is similar to a saddle-node one. Before the bifurcation, there is a pair of unstable fixed points, one of which corresponds by its nature to the fixed point in the Lorentz model and has one unstable and two stable directions, and the other has two unstable and one stable direction. As a parameter is varied, the points approach each other, coalesce at bifurcation, and disappear. In this case, the Lorentz attractor is realized at the parameter values on one side of the bifurcation point. On the other side, because of the disappearance of the fixed points, one of two variants is realized, depending on the structure of the vector field in remote domains visited by the trajectories. The first variant consists in the emergence of nonhyperbolic dynamics, and the second in the appearance of a Plykin-type attractor in the Poincaré map.

Because the Lorentz model is relevant for a number of physical systems, the version with a hyperbolic attractor is likely to be applicable to certain modifications of these systems.

An approach to constructing a two-dimensional map with a Plykin-type attractor in terms of explicit formulas was proposed in [53], where the question of the degree of the polynomials representing such a map was addressed. In fact, an example considered there involves functions that are compositions of polynomials through the 9th degree, and hence the resulting representation contains polynomials of a very high order (greater than 10^5). The author of Ref. [53] argues, however, that the lower bound on the order of polynomials that specify a map containing the Plykin attractor is equal to 7.

The Plykin attractor can be obtained starting from the DA attractor of Smale [20, 54]. The first step consists of introducing an additional symmetry, such that the image of the attractor is composed of four copies of the original attractor (as in the left part of Fig. 8). For this, taking the

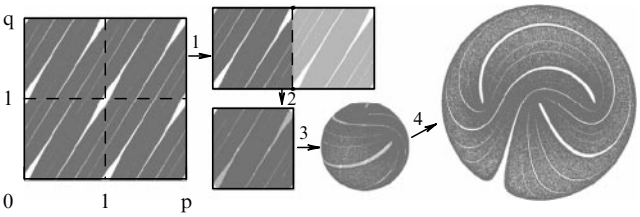

Figure 8. Illustration of transformations that allow passing from a DA attractor on a torus (left) to a Plykin attractor (right): 1 — selection of a rectangle that makes up half of a square, 2 — folding it, 3 — passing to a sphere using transformations in terms of the Weierstrass function, and 4 — passing to the plane using a transformation of variables.

map $p_{n+1}=p_n+q_n+f(p_n,q_n)$, $q_{n+1}=p_n+2q_n+g(p_n,q_n)$ obtained via surgery, we expand the definition domain to the square with side 2, and let this square represent an unrolled torus. This implies that the quantities p and q are assumed to be defined modulo 2, while the functions f and g are chosen as previously, i.e., their arguments are regarded as defined modulo 1. We now perform steps 1–4 (see Fig. 8). We take the upper or the lower half of the square (step 1). Viewing the picture as drawn on a transparent film, we fold it along the vertical middle line and glue along the left, top, and bottom edges (step 2). Because of the symmetry, the fibers of the attractor are connected accurately and correctly when glued. Further, we inflate the obtained square 'envelope' like a balloon, turning it into a sphere (step 3). Because the 2×2 square represents an unrolled torus, the variable transformation should be expressible in terms of a doubly periodic function of the complex variable $Z=p+\mathrm{i}q$ with periods 2 and $2i$, like the elliptic Weierstrass function $\wp$ [55]. Namely, the transformation to the Cartesian coordinates x, y, z of points on a unit sphere is defined by the relations $x+\mathrm{i}y=2\wp(Z)/\left(1+\left|\wp(Z)\right|^2\right)$ and $z=\left(1-\left|\wp(Z)\right|^2\right)/\left(1+\left|\wp(Z)\right|^2\right)$. Performing one more transformation of variables, we can pass from the sphere to a plane (step 4).[10] This results in a map with the attractor shown in Fig. 4b. The analytic representation of the map is rather cumbersome. In practice, it is certainly simpler to follow the iterations in the variables p and q, and use the above changes of variables for mapping the coordinates on the plane. The image of the attractor on the plane is shown in the right part of Fig. 8. The question about suspension in the framework of this construction is far from trivial, as was discussed in the thesis by Hunt [54], and an explicit transition to a system with continuous time was not performed.

Hunt's thesis [54] implements an alternative approach to constructing the suspension to a Plykin attractor. A system is defined in terms of differential equations in two variables, $\dot{x}=f_*(x,y,t)$ and $\dot{y}=g_*(x,y,t)$, where f_* and g_* are continuously differentiable functions, periodic in their argument t. They are defined differently at the three stages that make up the full period over which the right-hand sides change in time. The mathematical relations vary from one phase space domain to another and contain numerous smoothing functions introduced in an artificial way (for a detailed description and explanation, see Refs [54, 56]). The hyperbolicity of an

[10] Interestingly, the correspondence between points on a sphere and a torus, used in the reasoning above, was employed in cartography: it underlies the Guyou projection through which Earth's surface is mapped on a plane in the form of a periodically repeating picture that corresponds to unrolling the torus.

attractor in this model admits a rigorous mathematical substantiation, but the entire construction is so cumbersome that it is hardly reproducible in a physical device. The Hunt system was used in [56] to elaborate on computational methods of analyzing the dynamics on a hyperbolic attractor. The authors present and discuss the results of computer simulations of the dynamics and also mention and correct a technical error in a program contained in Hunt's work.

In [54, 57], the hyperbolic nature of the dynamics was established for a mechanical system involving the hinge mechanism discussed previously in a popular-science article [58] (Fig. 9). The ends of three identical rods are attached to three joints fixed at the vertices of an equilateral triangle, enabling the rods to rotate freely. Each rod on its other end hosts a movable joint through which it is attached to one of three other rods. These are connected together through a movable joint. Owing to the presence of constraints, only two of the angular variables that specify the instantaneous position of the rods are independent, i.e., the motion in the configuration space is constrained to a two-dimensional manifold. Topologically, it represents a genus-three surface (a pretzel with three holes, or triple torus). In the absence of friction and external forces, the motion is inertial and its kinetic energy is conserved. The kinetic energy is expressed as a quadratic form in the generalized velocities — time derivatives of local coordinates on the two-dimensional manifold. This quadratic form, whose coefficients depend on the relation between the length and masses of the construction, defines a metric on the two-dimensional manifold, and the motion follows the geodesic lines of this metric. By searching through variants, a set of parameters has been identified such that the metric is everywhere characterized by negative curvature. In this situation, as is well known, hyperbolic chaos in its conservative version occurs. The authors of Ref. [57] argue that by adding dissipation and a negative feedback mechanism, a system with a hyperbolic attractor can be obtained; however, the research that would demonstrate such an attractor on the level of computer-aided modeling or in experiment is lacking thus far.

It was noted in [59] that a hyperbolic attractor is realizable in the Hindmarsh–Rose model of the neuron. This model is described by an autonomous system of third-order equations $\dot{x}=y-x^3+3x^2-z$, $\dot{y}=1-5x^2-y$, and $\dot{z}=\mu\big[4(x-x_0)-z-\delta\big]$, where δ, μ, and x_0 are parameters [60]. For fixed μ and x_0 (for example, $\mu=0.003$ and $x_0=-1.6$), the model is capable of demonstrating various regimes depending on the parameter δ. In the domain $\delta<\delta_1$, slow auto-oscillations, or burst activity according to the accepted terminology, are realized; in the domain $\delta>\delta_2$, fast periodic oscillations are observed, referred to as spike generation. In the intermediate range, $\delta_1<\delta<\delta_2$, the spikes are present on the burst background, and it is precisely this interval of parameters where nontrivial dynamical phenomena are possible. The authors of Ref. [59] start with a formal generalized form of equations $\dot{\mathbf{x}}=\mathbf{X}(\mathbf{x},z)$ and $\dot{z}=\mu\big[Z(\mathbf{x})-z-\delta\big]$, where $\mathbf{x}$ is a two-dimensional vector and the functions $\mathbf{X}(\mathbf{x},z)$ and $Z(\mathbf{x})$ are specified only to the degree necessary to justify the proposed qualitative arguments. According to the analysis, in the domain of transition from the periodic spike generation to burst activity, a situation might occur where a two-dimensional Poincaré map is defined on a disk with three 'holes,' paving the road to the Plykin attractor. These results are interesting because they are, in a certain sense, obtained for the model of natural origin, and are indicative of a possible role of hyperbolic dynamics in neuronal networks. Admittedly, no specific research that would elaborate on the explicit form of the equations and demonstrate a hyperbolic attractor via numerical simulation has been proposed yet.

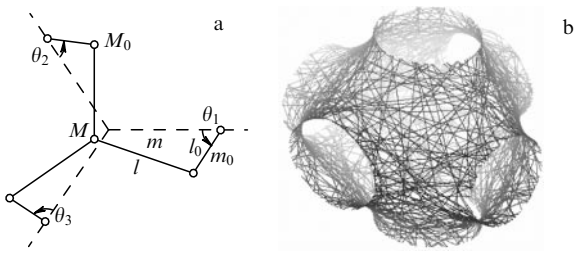

Figure 9. Mechanical system: the hinge mechanisms of Thurston and Weeks with chaotic dynamics (a) and a trajectory in the three-dimensional space $(\theta_1, \theta_2, \theta_3)$ obtained in numerical simulations for lengths and masses $l=41/40$, $l_0=7/40$, $m=9/100$, $M=13/100$, $M_0=1/5$, and $m_0=0$ (b).

The possibility of the occurrence of the Smale–Williams attractor in the context of the so-called blue sky catastrophe was substantiated in [61, 62]. In its simplest form, the blue sky catastrophe is encountered in a three-dimensional autonomous system. There is a saddle–node periodic orbit in the phase space at the moment of bifurcation, and the system departs from it along trajectories forming a 'tube' that narrows and, spiraling, approaches the same saddle-node orbit from the opposite side. Upon shifting to one side with respect to the parameter, the saddle-node cycle is replaced by a pair of limit cycles: one is unstable, and the other corresponds to a stable auto-oscillating regime. Upon shifting to the other side, the saddle-node cycle vanishes, leaving an agglomeration formed by loops of the spiraling trajectory, which represents a part of the attracting limit cycle that had emerged instead of a 'tube.' For the initial angular coordinate φ, the trajectory, having completed the path along the tube, returns to the saddle-node cycle with the angular coordinate whose expression contains the term $m\varphi$ in the general case. For three-dimensional systems, only the $m=0$ or $m=1$ cases can occur, but beginning from dimension four, the integer number m can be arbitrary. In particular, if $m=2$, the toroidal domain in a section in the vicinity of the saddle-node cycle on its unstable side transforms on return into a folded loop, such that the bifurcation is accompanied by the appearance of the Smale–Williams attractor.

Examples pertaining to the blue sky catastrophe in the literature were limited until recently to systems with a three-dimensional phase space [63–65], in which the transition to the Smale–Williams attractor is impossible. A system of fourth-order differential equations allowing such an attractor was recently proposed in Ref. [66] (see also Section 9.2).

An amusing example illustrating that it is possible to deform a cloud of representing points without discontinuities and local compactions, as required for a hyperbolic attractor, is offered by the machine for stretching and folding sugar taffy (taffy-pulling machine). The rotational motion of transverse rods enforces continuous stretching and folding of taffy from treacle and sugar, accompanied by formation of a fine transverse fiber structure.[11] In [67], a mathematical

[11] The reader may find pictures and movies illustrating the operation of such a machine on the Internet; the keywords needed for the search are 'taffy-pulling machine.'

model is proposed in the form of a map that describes the dynamics of a substance subjected to transformations. Notably, such a machine cannot be regarded as a variant of the physical implementation of a hyperbolic attractor in the sense implied in the context of this review. Indeed, it does not belong to low-dimension dynamical systems but pertains to deformations of a continuous medium, and the map of the relevant type derives from the description of displacements of separate elements. This is the dynamics of a real substance in physical space, and not the dynamics of phase fluid in its phase space.

In can be assumed that some of the approaches listed here may appear useful in delineating directions in the further search for physically realizable systems with hyperbolic attractors.

7. The Smale–Williams solenoid in the problem of particle motion on a plane under pulse-periodic action

There are numerous physical systems for which the description of their dynamics in terms of discrete time appears intuitive and highly natural. This pertains, for example, to mechanical systems when motion forced by a sequence of periodic pulses is considered and a map dealing with the state change between two subsequent pulses is derived. In particular, the maps by Zaslavsky, Hénon, and Ikeda came to be known in this context [3, 11, 69, 70].

We turn to a problem involving a map with the Smale–Williams hyperbolic attractor [71, 72]. We consider the motion of a unit mass particle on the plane (x, y) in the presence of friction proportional to velocity. Let the motion occur in the potential field $U(x,y) = -(1/2)\,\mu(x^2+y^2)+(1/4)\,\mu(x^2+y^2)^2$, which has the rotational symmetry with respect to the origin and a minimum on the unit circle. We assume that an additional forcing field is applied for a short time interval periodically with a period T, such that the particle gains a momentum $\mathbf{P}(x,y) = (P_x(x,y),\ P_y(x,y))$ whose direction and amplitude depend on the instantaneous particle position. Setting the friction coefficient to unity for simplicity, we write the equations

$$\begin{aligned} \ddot{x} + \dot{x} &= \mu x(1 - x^2 - y^2) + P_x(x,y) \sum_{n=-\infty}^{\infty} \delta(t - nT)\,, \\ \ddot{y} + \dot{y} &= \mu y\,(1 - x^2 - y^2) + P_y(x,y) \sum_{n=-\infty}^{\infty} \delta(t - nT)\,. \end{aligned} \tag{1}$$

The spatial distribution of the forcing field $\mathbf{P}(x,y)$ is selected from the following consideration. We assume that there is a ring of particles at rest on a unit circle, with coordinates $x = \cos\varphi$ and $y = \sin\varphi$. Following a stimulus from the force field, each particle initially characterized by an angle φ acquires the momentum with components $P_x(x,y)$ and $P_y(x,y)$, which leads to a change in the particle coordinates with time. In the absence of a potential field, the particle comes to rest at the point with the coordinates

$$x' = x + P_x(x,y)\,, \quad y' = y + P_y(x,y)\,. \tag{2}$$

We require that the particles be again arranged over the unit circle but such that the cycle around the original circle corresponds to two or three cycles for the new arrangement, i.e., that the angular coordinate undergoes the transformation $\varphi' = M\varphi \pmod{2\pi}$, where $M = 2$ or 3. For this, the new particle coordinates must be expressed as

$$x' = \cos\varphi' = \cos M\varphi\,, \quad y' = \sin\varphi' = \sin M\varphi\,, \tag{3}$$

and the functions characterizing the distribution of the forcing field should be chosen such that

$$\begin{aligned} P_x(x,y) &= x' - x = \cos M\varphi - \cos\varphi\,, \\ P_y(x,y) &= y' - y = \sin M\varphi - \sin\varphi\,. \end{aligned} \tag{4}$$

Using the relation between the Cartesian and angular coordinates on the unit circle, $x = \cos\varphi$ and $y = \sin\varphi$, and some trigonometric formulas, we can show that the desired result is obtained by setting

$$P_x(x,y) = 2x^2 - x - 1\,,\ P_y(x,y) = 2xy - y \ \text{ for } M = 2\,, \tag{5}$$

$$P_x(x,y) = 4x^3 - 4x\,,\ P_y(x,y) = -4y^3 + 2y \ \text{ for } M = 3\,. \tag{6}$$

(We note that the pulse force field is potential in the second case. Its x and y components are functions of only the respective coordinate. This can be considered an advantage of this version of the model from the standpoint of its implementation.)

We assume the parameter μ to be sufficiently small such that the displacement in the potential field $U(x,y)$ for the characteristic time associated with the action is small. On the other hand, we select the time interval between the pulses T to be sufficiently large such that the particle can approach the minimum of the potential field. These conditions are not too restrictive and it is sufficient if they hold in some rough approximation.

Having specified the initial state just before the nth pulse, $\mathbf{x}_n = \{x, \dot{x}, y, \dot{y}\}_{t=nT-0}$, and integrating equations (1) over the period T, we can determine the state before the next pulse. Accordingly, the description of the dynamics is reduced to considering the four-dimensional map $\mathbf{x}_{n+1} = \mathbf{f}(\mathbf{x}_n)$.

A topological property of the particle ensemble under the transformation, namely, the emergence of a configuration encircling the origin two or three times, is essential for the implementation of the Smale–Williams attractor. Contraction in the transverse direction in the phase space is ensured by friction and the action of potential fields owing to which the particle moves toward the unit circle, where the potential has a minimum. Unlike in the classical Smale–Williams construction, the attractor in this case is embedded in a four-dimensional, not three-dimensional, space.

Illustrations obtained by numerically solving the equations of motion are shown in Fig. 10a–c for $M = 2$ and in Fig. 10d–f for $M = 3$, for the pulse field distributions defined by expressions (5) and (6). The portraits of the attractors in the projection on the (x, y) plane in a stroboscopic section that corresponds to the instant just before the next pulse are shown in Fig. 10a and d; the magnified insets help visualize the transverse fractal structure of the attractors. The apparent correspondence with the Smale–Williams solenoid is obvious. Shown is the iteration diagram for the angular coordinate $\varphi = \arg(x + \mathrm{i}y)$ computed just before the next pulse. As can be seen, the map of the angular coordinate is of the same topological type as the Bernoulli map: the single path along the circle for the preimage corresponds to the twofold (Fig. 10b) or threefold (Fig. 10e) cycle for the image. Also

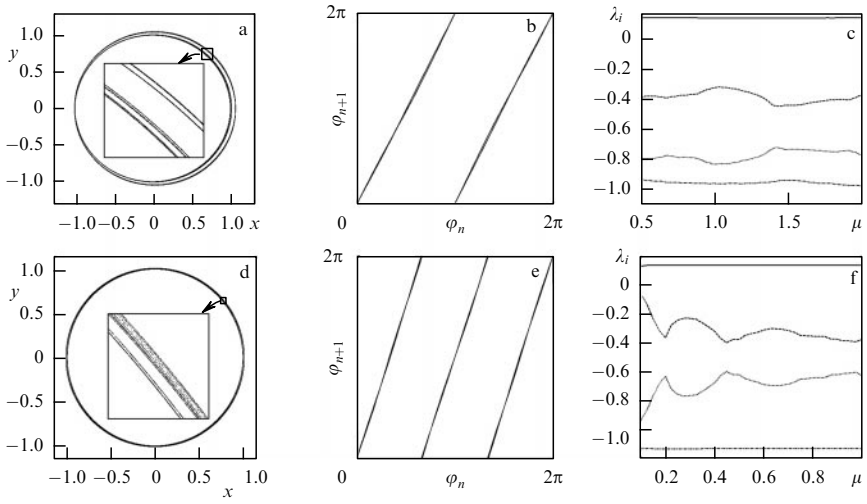

Figure 10. Portraits of attractors in a stroboscopic section (a, d). Iteration diagrams for the angular coordinate obtained by numerically solving the equations (b, e). The dependence of four Lyapunov exponents on the parameter μ (c, f). The results are given for system (1), with the distribution of the pulse force field specified by expressions (5) (diagrams a–c) and (6) (diagrams d–f). For the first series of diagrams, $T = 5$, and for the second, $T = 8$. The plots in diagrams a and b correspond to $\mu = 0.44$, and the plots in diagrams d and e correspond to $\mu = 0.22$.

shown are plots of the Lyapunov exponents as functions of the parameter μ for a fixed period of pulse repetition. As can be seen, for a wide range of μ, the largest exponent of the stroboscopic map, Λ_1, stays almost constant, and is in good agreement with the estimate $\Lambda_1 \approx \ln 2$ for the first case (Fig. 10c) and $\Lambda_1 = \ln 3$ for the second (Fig. 10f). This is in line with the values of exponents for the one-dimensional Bernoulli map, which approximately describes the dynamics of the angular coordinate. The other Lyapunov exponents are negative. The estimates of the fractal dimension of the attractors depicted in Fig. 10a and d respectively give $D = 1.328$ and $D = 1.47$.

8. Uniformly hyperbolic attractors in differential equations with piecewise right-hand sides continuous in time

One way of designing a nonautonomous system whose stroboscopic map contains a uniformly hyperbolic attractor consists in enforcing its time evolution to follow a sequence of periodically repeating stages, such that the governing differential equations are defined differently at each stage. Such an approach was used in [54] to construct the suspension to a Plykin-type attractor. A simpler model with an attractor of the same type is considered in Section 8.1.

It should be remembered that a Plykin-type attractor can be regarded as located on a plane or a sphere because of the correspondence between points of the sphere and of the plane via the stereographic projection. In Section 8.1, we analyze the dynamics determined by a certain sequence of continuous transformations on a sphere, which ensures the presence of a Plykin attractor [73, 74]. In Section 8.2, we demonstrate how such dynamics can be implemented in a nonautonomous system of coupled oscillators [75].

8.1 A dynamical system with a Plykin-type attractor

We construct a dynamical system whose instantaneous states correspond to points on the unit sphere and are specified by variables x, y, and z subject to the condition $x^2 + y^2 + z^2 = 1$ (Fig. 11a). The role of 'holes' that are necessary for a Plykin attractor to exist is played by neighborhoods of points labeled as A, B, C, and D in the figure. We let N and S denote the northern and southern poles. We consider a sequence of continuous transformations performed one after another, each of a unit duration in time, and obeying the differential equations given below.

I. *Shift along parallels*, i.e., displacement of representing points on the sphere from meridians NABS and NCDS along parallels to an equidistant meridional circle:

$$\dot{x} = -\varepsilon x y^2\,, \quad \dot{y} = \varepsilon x^2 y\,, \quad \dot{z} = 0\,. \tag{7}$$

II. *Differential rotation around the z axis* with an angular velocity that linearly depends on z such that points on parallel BC stay at rest and those on parallel AD are rotated through 180°:

$$\dot{x} = \pi\left(\frac{z}{\sqrt{2}} + \frac{1}{2}\right) y\,, \quad \dot{y} = -\pi\left(\frac{z}{\sqrt{2}} + \frac{1}{2}\right) x\,, \quad \dot{z} = 0\,. \tag{8}$$

III. *Shift to the equator*, i.e., displacement of representing points along circles centered on the x axis on the sphere from the large circle ABCD to the equator:

$$\dot{x} = 0\,, \quad \dot{y} = \varepsilon y z^2\,, \quad \dot{z} = -\varepsilon y^2 z\,. \tag{9}$$

IV. *Differential rotation around the x axis* with an angular velocity that linearly depends on x such that the plane section orthogonal to the x axis and containing point C stays at rest and the section containing point B turns through 180°:

$$\dot{x} = 0\,, \quad \dot{y} = -\pi\left(\frac{x}{\sqrt{2}} + \frac{1}{2}\right) z\,, \quad \dot{z} = \pi\left(\frac{x}{\sqrt{2}} + \frac{1}{2}\right) y\,. \tag{10}$$

Intuitively, it seems rather plausible that such a sequence of transformations generates a flow on the sphere that forms a layered structure characteristic of Plykin attractors. We mention the symmetry inherent in the problem: stages I and II differ from III and IV only by the permutation of x and z.

Differential equations for each of the stages can be solved analytically. As a result, we obtain the map for the full period

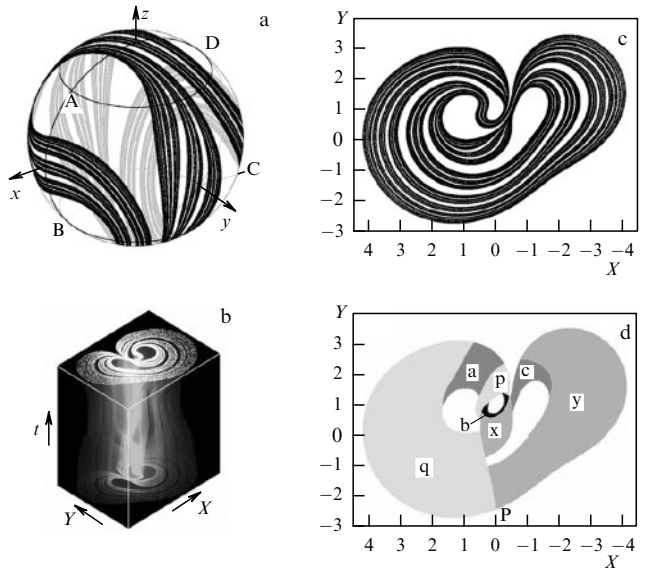

Figure 11. The attractor of map (11) for $\varepsilon = 0.77$ on the unit sphere (a), the attractor of differential equation system (14) in the augmented phase space (b), the portrait of an attractor in the Poincaré section in the plane of variables X and Y (c), and the Markov partition of the absorbing domain (d). The graph defining the grammar rules and notation of the elements of the Markov partition are analogous to those in Fig. 7b. To facilitate comparison, the direction of the horizontal axis in diagrams c and d is inverted. (Animations showing the transformations on a sphere and in a plane in continuous time can be found at http://www.sgtnd.narod.ru/science/hyper/eng/index.htm.)

as a system of maps that correspond to all four stages:

$$\mathbf{x}_{n+1} = \mathbf{f}_+\big(\mathbf{f}_-(\mathbf{x}_n)\big), \mathbf{f}_\pm(\mathbf{x})$$

$$= \begin{pmatrix} \pm z \\ \dfrac{y \exp[\varepsilon/2(x^2+y^2)] \cos(\pi/2)(z\sqrt{2}+1)}{\sqrt{\cosh \varepsilon(x^2+y^2) + \varepsilon(y^2-x^2)\,[\varepsilon(x^2+y^2)]^{-1} \sinh \varepsilon(x^2+y^2)}} \\ \pm \dfrac{x \exp[-\varepsilon/2(x^2+y^2)] \sin(\pi/2)(z\sqrt{2}+1)}{\sqrt{\cosh \varepsilon(x^2+y^2) + \varepsilon(y^2-x^2)\,[\varepsilon(x^2+y^2)]^{-1} \sinh \varepsilon(x^2+y^2)}} \\ \dfrac{y \exp[\varepsilon/2(x^2+y^2)] \sin(\pi/2)(z\sqrt{2}+1)}{\sqrt{\cosh \varepsilon(x^2+y^2) + \varepsilon(y^2-x^2)\,[\varepsilon(x^2+y^2)]^{-1} \sinh \varepsilon(x^2+y^2)}} \\ \mp \dfrac{x \exp[-\varepsilon/2(x^2+y^2)] \cos(\pi/2)(z\sqrt{2}+1)}{\sqrt{\cosh \varepsilon(x^2+y^2) + \varepsilon(y^2-x^2)\,[\varepsilon(x^2+y^2)]^{-1} \sinh \varepsilon(x^2+y^2)}} \end{pmatrix}. \tag{11}$$

We note that point C serves as an (unstable) fixed point on the map and points A, B, and D form an unstable cycle of period 3 (A → D → B → A).

Figure 11a depicts the attractor of map (11) on the sphere for $\varepsilon = 0.77$. We mention that the attractor shows the characteristic transverse fractal structure, looking as if it were composed of strips each containing the strips of the next level. The Lyapunov exponents of the attractor for the selected parameters are found to be $\Lambda_1 = 0.959$ and $\Lambda_2 = -1.141$, and the dimension of the attractor according to the Kaplan–Yorke formula is $D_L \approx 1 + \Lambda_1/|\Lambda_2| = 1.841$.

The description of the dynamics can be reformulated such that the instantaneous states are represented by points on the plane. For this, perform the variable transformation

$$W = X + \mathrm{i}Y = \frac{x - z + \mathrm{i}y\sqrt{2}}{x + z + \sqrt{2}}, \tag{12}$$

which corresponds to the stereographic projection with the projection center at point C. (This point stays inside the 'hole' during all stages, and hence the attractor image on the plane occupies a finite domain.)

The equations that describe the dynamics in continuous time take the following form in the variables X and Y:

$$\dot{X} = F(X, Y, t), \quad \dot{Y} = G(X, Y, t), \tag{13}$$

where

$$\begin{aligned} F(X,Y,t) = {} & \frac{\pi}{\sqrt{2}}\, Y \frac{(1-X)^2 s_2 - (1+X)^2 s_4}{1+X^2+Y^2} \\ & + \varepsilon Y^2 \left[\frac{(1+2X-X^2-Y^2)(X-1)\, s_1}{(1+X^2+Y^2)^2} \right. \\ & \left. + \frac{(1-2X-X^2-Y^2)(X+1)\, s_3}{(1+X^2+Y^2)^2} \right], \end{aligned}$$

$$\begin{aligned} G(X,Y,t) = {} & \frac{\pi}{\sqrt{2}} \left[\frac{(X-1)(1+2X-X^2+Y^2)\, s_2}{2(1+X^2+Y^2)} \right. \\ & \left. - \frac{(X+1)(1-2X-X^2+Y^2)\, s_4}{2(1+X^2+Y^2)} \right] + \\ & + \varepsilon Y \left[\frac{(1+2X-X^2-Y^2)(1+2X-X^2+Y^2)\, s_1}{2(1+X^2+Y^2)^2} \right. \\ & \left. + \frac{(1-2X-X^2-Y^2)(1-2X-X^2+Y^2)\, s_3}{2(1+X^2+Y^2)^2} \right], \end{aligned} \tag{14}$$

$$s_k(t) = \begin{cases} 1, & k-1 \leqslant t - 4\left\lfloor \dfrac{t}{4} \right\rfloor < k, \\ 0, & t - 4\left\lfloor \dfrac{t}{4} \right\rfloor < k-1, \quad t - 4\left\lfloor \dfrac{t}{4} \right\rfloor \geqslant k. \end{cases}$$

Figure 11b displays the portrait of the attractor of the system of differential equations (14) in the three-dimensional augmented phase space.[12] (The pattern invites associations with rising clouds of smoke.) In the section by a horizontal plane, there is an object shown separately in Fig. 11c. This is none other than the attractor of map (11) in coordinates defined in terms of transformation (12).

As follows from a thorough analysis of filament positions, the attractor in the Poincaré section belongs to the same type as the attractor shown in Fig. 4b. The hyperbolic nature of the attractor is confirmed by numerically verifying the cone criterion [74] and by the analysis of positions of stable and unstable manifolds in the Poincaré section based on numerical simulations [74, 75]. Figure 11d shows the Markov partition of the absorbing domain containing the attractor. The boundary between the partition domains is given by the stable manifold of fixed point P. Comparing this diagram

[12] From a formal standpoint, it may seem that system (13) is not fully satisfactory as a suspension because the equations contain time-discontinuous functions $s_k(t)$. However, on the one hand, this does not hamper the presence of a uniformly hyperbolic attractor in the stroboscopic map which represents a composition of diffeomorphisms; on the other hand, the model allows modifications such that the dependence of coefficients on time becomes smooth. In this case, due to to structural stability, the nature of the attractor is preserved in a stroboscopic map (the respective modification is suggested in Ref. [73]).

with Fig. 7b, we once again see that this attractor and the one of the Plykin type in Fig. 4b are topologically equivalent. The partition domains are labeled with letters such that the grammar rules for symbolic description of the dynamics correspond to the graph in Fig. 7b.

8.2 A model with a Plykin-type attractor based on coupled oscillators

We turn to a system of two auto-oscillating elements that compensate their energy loss from a common source. The system is defined by the equations

$$\begin{aligned}\dot{a} &= \frac{1}{2}\,\mu\bigl(1-|a|^2-|b|^2\bigr)\,a\,,\\ \dot{b} &= \frac{1}{2}\,\mu\bigl(1-|a|^2-|b|^2\bigr)\,b\,,\end{aligned} \tag{15}$$

where a and b are the complex-valued amplitudes and μ is a positive parameter. Clearly, the stationary regime of auto-oscillations corresponds to the fulfillment of the condition $\rho \equiv |a|^2+|b|^2=1$. If we regard the system states differing only by their common phase as indistinguishable, i.e., consider states (a,b) and $(a\exp(\mathrm{i}\phi),\, b\exp(\mathrm{i}\phi))$ equivalent, then the states satisfying $\rho=1$ can be associated with points on the unit sphere, such that the relation to the coordinates x, y, and z satisfying the condition $x^2+y^2+z^2=1$ is given by

$$x+\mathrm{i}y = 2a^*b\,,\quad z=|a|^2-|b|^2\,. \tag{16}$$

We modify model (15) to obtain a system of equations whose coefficients periodically vary in time such that its Poincaré map representing states on the sphere contains the same attractor as in Section 8.1. For this, we introduce a sequence of continuous transformations on the sphere, which, taken together, are equivalent to the transformations considered above. To simplify the representation of equations in terms of complex amplitudes, we assume that the process evolves in six stages [75].

I. *Shift along parallels*:

$$\dot{a} = -\mathrm{i}\varepsilon a\,\mathrm{Im}\,(a^*b)^2\,,\quad \dot{b} = \mathrm{i}\varepsilon b\,\mathrm{Im}\,(a^*b)^2\,. \tag{17}$$

II. *Differential rotation around the z axis:*

$$\begin{aligned}\dot{a} &= -\frac{1}{4}\,\mathrm{i}\pi\bigl(\sqrt{2}-1-2\sqrt{2}\,|a|^2\bigr)\,a\,,\\ \dot{b} &= -\frac{1}{4}\,\mathrm{i}\pi\bigl(\sqrt{2}+1-2\sqrt{2}\,|b|^2\bigr)\,b\,.\end{aligned} \tag{18}$$

III. *Rotation through* 90° *around the y axis*:

$$\dot{a} = -\frac{1}{4}\,\pi b\,,\quad \dot{b} = \frac{1}{4}\,\pi a\,. \tag{19}$$

IV. *Shift along parallels*:

$$\dot{a} = -\mathrm{i}\varepsilon a\,\mathrm{Im}\,(a^*b)^2\,,\quad \dot{b} = \mathrm{i}\varepsilon b\,\mathrm{Im}\,(a^*b)^2\,. \tag{20}$$

V. *Reversed differential rotation*:

$$\begin{aligned}\dot{a} &= \frac{1}{4}\,\mathrm{i}\pi\bigl(\sqrt{2}-1-2\sqrt{2}\,|a|^2\bigr)\,a\,,\\ \dot{b} &= \frac{1}{4}\,\mathrm{i}\pi\bigl(\sqrt{2}+1-2\sqrt{2}\,|b|^2\bigr)\,b\,.\end{aligned} \tag{21}$$

VI. *Reversed rotation around the y axis*:

$$\dot{a} = \frac{1}{4}\,\pi b\,,\quad \dot{b} = -\frac{1}{4}\,\pi a\,. \tag{22}$$

The procedure is symmetric in the sense that the transformations at stages I and IV are identical, while stages II and III differ from V and VI only by the direction of rotation.

Let the initial conditions for Eqns (17) at the instant $t_n = nT$ correspond to a state vector $\mathbf{X}_n = (a_n, b_n)$. The equations can be solved analytically at stages I–VI, with the map then taking the explicit form

$$\mathbf{X}_{n+1} = \mathbf{F}_+\bigl(\mathbf{F}_-(\mathbf{X})\bigr),\ \mathbf{F}_\pm(\mathbf{X}) = \begin{pmatrix} \left\{ \dfrac{aD\exp\left[\pm(\mathrm{i}\pi/4)(\sqrt{2}-1-2\sqrt{2}\,|a|^2)\right]}{\sqrt{1+(|a|^2+|b|^2)(\exp(\mu)-1)}} \right. \\ \left. \mp \dfrac{bD^*\exp\left[\pm(\mathrm{i}\pi/4)(\sqrt{2}+1-2\sqrt{2}\,|b|^2)\right]}{\sqrt{1+(|a|^2+|b|^2)(\exp(\mu)-1)}} \right\} \exp\dfrac{\mu}{2} \\ \left\{ \dfrac{\pm aD\exp\left[\pm(\mathrm{i}\pi/4)(\sqrt{2}-1-2\sqrt{2}\,|a|^2)\right]}{\sqrt{1+(|a|^2+|b|^2)(\exp(\mu)-1)}} \right. \\ \left. + \dfrac{bD^*\exp\left[\pm(\mathrm{i}\pi/4)(\sqrt{2}+1-2\sqrt{2}\,|b|^2)\right]}{\sqrt{1+(|a|^2+|b|^2)(\exp(\mu)-1)}} \right\} \exp\dfrac{\mu}{2} \end{pmatrix}, \tag{23}$$

where

$$D(a,b) = \frac{1}{\sqrt{2}}\left[\frac{|a|^2|b|^2-(a^*b)^2\tanh(2\varepsilon|a|^2|b|^2)}{|a|^2|b|^2-(ab^*)^2\tanh(2\varepsilon|a|^2|b|^2)}\right]^{1/4}. \tag{24}$$

The dynamics governed by Eqns (18)–(22) or map (24) is unchanged when the phases of the oscillators are simultaneously shifted by the same constant, i.e., is invariant under the transformation $a\to a\exp(\mathrm{i}\psi)$, $b\to b\exp(\mathrm{i}\psi)$. This allows passing from two equations for two complex amplitudes to three equations for real-valued variables by performing the change of variables in (16). In this representation, the map is three-dimensional, the unit sphere represents an invariant set, and the quantity $\rho\equiv x^2+y^2+z^2$ tends to 1 as the number of iterations increases. On the unit sphere $\rho=1$, the map for the variables x, y, and z is just equivalent to (11).

Figure 12a plots the time dependence of the amplitudes $|a|$ and $|b|$ of two oscillators obtained by solving the differential equations numerically. Small in amplitude and random in phase, complex-valued a and b are taken as initial conditions, and hence the plots correspond to a transient process of the development of chaotic auto-oscillations. In their right part, the dependences resemble realizations of a random process, as expected from the dynamics on a chaotic attractor. Their local structure bears imprints of the specific character of the dynamics composed of subsequent stages. In particular, the horizontal intervals, the plateaus, correspond to stages I, II, IV, and V of the evolution, during which the amplitudes $|a|$ and $|b|$ remain constant. Figure 12b shows the attractor in the stroboscopic section that corresponds to the time instants $t_n = nT$, $T=6$. To visualize the transverse Cantor structure inherent in the attractor, the coordinates $\mathrm{Re}(a^*b)$, $\mathrm{Im}(a^*b)$ are used for the presentation. The points are plotted in dark color if the amplitude of the first oscillator exceeds that of the

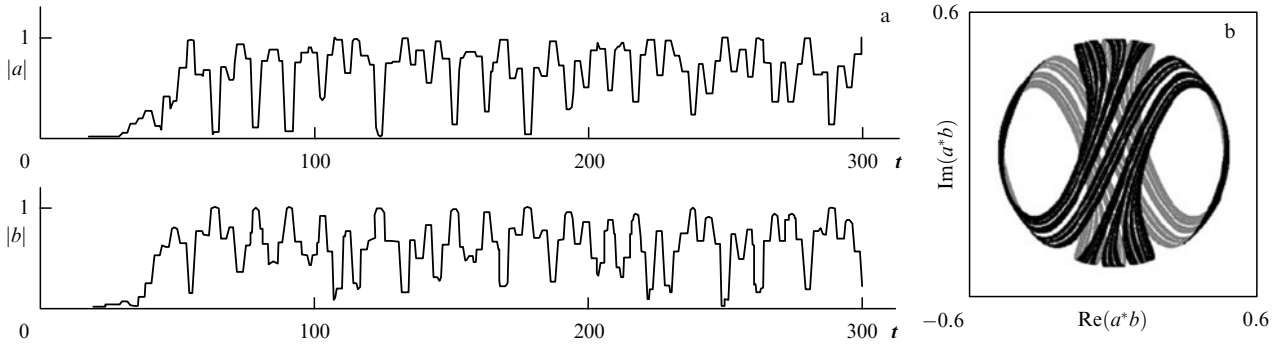

Figure 12. (a) Time dependences of the amplitudes $|a|$ and $|b|$ of two oscillators in the process of establishing the chaotic oscillation regime, obtained by numerically solving differential equations (17)–(22). (b) Portrait of the attractor in a stroboscopic section with $\varepsilon = 0.77$ and $\mu = 1$.

second at the given instant of time, and in light color otherwise. As can be seen from formulas (16), this way of presentation corresponds to a particular planar projection of the image of the attractor from the sphere. It can be verified that the attractor corresponds to that of the formal model considered in Section 8.1 (see Fig. 11). Two Lyapunov exponents for Poincaré map (23) coincide with those for map (11). Additionally, there is a zero exponent, related to perturbations involving a phase shift in both oscillators by the same value, and a negative exponent associated with the approach of the trajectories to the invariant sphere.

A remark is due here. In a system of equations for complex-valued amplitudes, the attractor cannot be directly interpreted as a uniformly hyperbolic one because of the presence of a neutral direction in the state space associated with the common phase. It should be classed with *partly hyperbolic attractors* [20, 26]. For the model considered here, the remark is of a rather formal character because the invariance under the phase shift is exact, and it is appropriate to treat the states that differ from each other by their common phase as indistinguishable. But in systems where the representation in terms of slowly varying complex-valued amplitudes serves only the goal of an approximate description, the specific features of a partly hyperbolic attractor may become noticeable. If corrections caused by deviations from the approximate description remain small, we may assume that the common phase experiences slow random walk, while the dynamics of the other variables preserve their character as the consequence of its inherent roughness.

Other situations are known in physics when states are naturally associated with points on a unit sphere. Examples are furnished by the representation of two-level systems, in particular, spin-1/2 particles, on the Bloch sphere [76] or the description of light polarization in terms of Stokes parameters [77]. It is not unlikely that performing some manipulations with these systems would allow implementing dynamics identified with a Plykin-type attractor.

9. Uniformly hyperbolic attractors in systems of coupled oscillators with alternating excitation

It was noted in [78] that a hyperbolic attractor can be realized in the system of two van der Pol oscillators, which alternately activate owing to modulation of a parameter responsible for the bifurcation leading to the birth of a limit cycle. The generation of oscillations in the oscillator as it enters its active phase is stimulated through the transfer of excitation from its partner, which occurs such that the phase variable increases twofold over the full excitation exchange cycle. The idea of manipulating the phase in the process of excitation exchange between alternately active partial oscillators proved to be a useful general principle enabling construction of examples of systems that realize the suspension of Smale–Williams attractors, and also systems that demonstrate a number of other phenomena with complex dynamics [79–83].

9.1 The Smale–Williams attractor in the system of coupled nonautonomous van der Pol oscillators

The principal requirement enabling the realization of a Smale–Williams attractor is the availability of a certain angular variable φ that is multiplied by two (or a larger integer) in iterations of the Poincaré map, whereas the phase volume contracts along all other directions in the state space. Let this variable be the phase of the oscillatory process. We construct a nonautonomous system such that a map with the required properties for the phase is realized over the period of the coefficient variation in the equations.

We consider two coupled van der Pol oscillators with frequencies ω_0 and $2\omega_0$, described by the equations

$$\ddot{x} - \left(A\cos\frac{2\pi t}{T} - x^2\right)\dot{x} + \omega_0^2 x = \varepsilon y\cos\omega_0 t\,,$$
$$\ddot{y} - \left(-A\cos\frac{2\pi t}{T} - y^2\right)\dot{y} + 4\omega_0^2 y = \varepsilon x^2\,. \qquad (25)$$

The generalized coordinates x and y are related to subsystems excited in turn due to enforced variation of the parameter with the period T, the modulation depth being controlled by the constant A. The coupling of the subsystems is characterized by the coupling parameter ε. The effect of the first oscillator on the second one is modeled with the term proportional to the squared generalized coordinate, and the effect of the second on the first is parameterized through the term containing the product of the generalized coordinate with the auxiliary basic signal with frequency ω_0. The relation $T = 2\pi N/\omega_0$, where N is an integer, is assumed to be satisfied, with the implication that system (25) has periodic coefficients.

We clarify the principle of system functioning. Let the first oscillator have the phase φ in its activity stage, with $x \sim \cos(\omega_0 t + \varphi)$. The action of the first oscillator on the second is determined by the second harmonic $\cos(2\omega_0 t + 2\varphi)$ with the phase 2φ. This harmonic corresponds to the frequency of the second oscillator and facilitates its excitation in the transition to the active stage. Notably, the arising oscillations acquire the same phase 2φ (up to a constant).

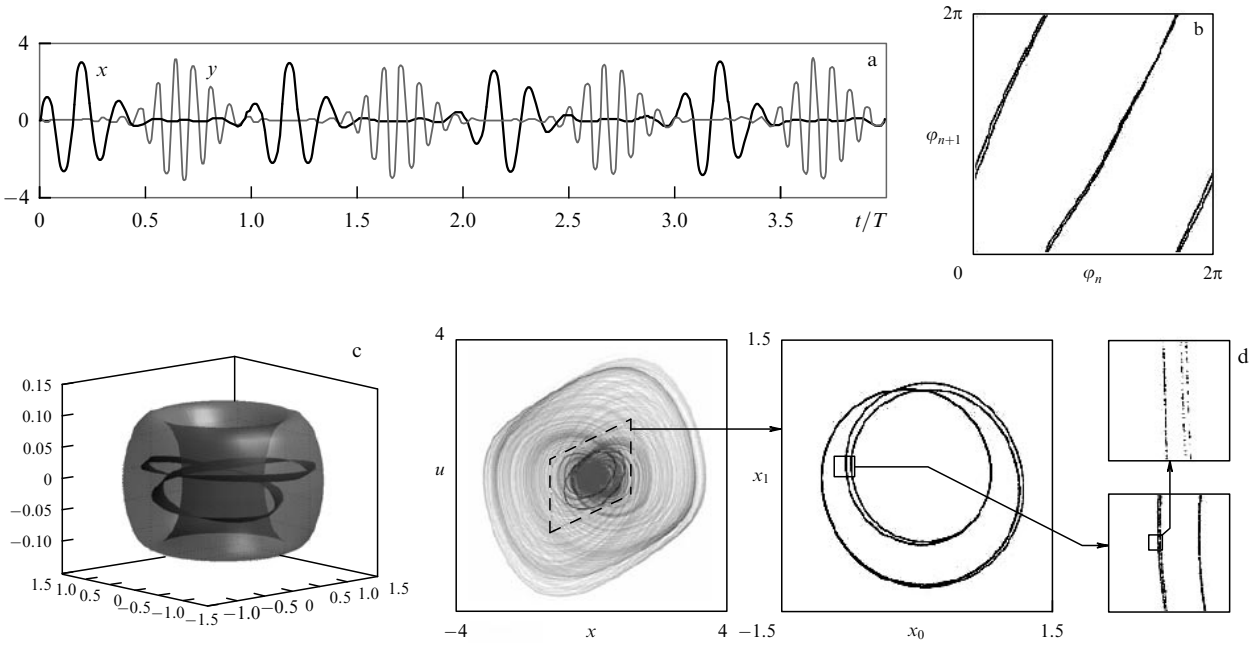

Figure 13. (a) Time dependence of variables x and y obtained by numerically solving Eqns (25) for $\omega_0 = 2\pi$, $T = 6$, $A = 5$, and $\varepsilon = 0.5$ (b) Diagram of the map for those phases related to the middle of excitation stages of the first oscillator. (c) Absorbing domain and its image under the action of a Poincaré map in the three-dimensional projection of space $\{x_0, x_1, x_2, x_3\} = \{x/0.812, (u - 0.438x)/0.721, y + 0.042x - 0.22u, v + 0.218x - 0.029u + 0.118y\}$. (d) Attractor of the system of coupled nonautonomous van der Pol oscillators in a projection on the phase plane of the first oscillator in the original variables; to the right: the portrait of the attractor in the Poincaré section on the plane (x_0, x_1).

In turn, when the second oscillator acts on the first one, due to the combination of oscillations of y with the auxiliary signal, a component with the frequency ω_0 with phase 2φ appears, which, being in resonance with the first oscillator, provides a seed for the oscillations with this phase at the oscillator next active stage.

Thus, both systems transfer the excitation from one to the other in turn, and at sequential activity stages the phase of the first oscillator, in the approximation considered here, is given by the Bernoulli map

$$\varphi_{n+1} = 2\varphi_n + \text{const} \pmod{2\pi} . \tag{26}$$

The additive constant occurs from the contributions to the phase as the excitation is transferred from one oscillator to the other, and can be eliminated by adjusting the reference point of φ.

The process described above is indeed observed in numerical simulations of the dynamics of system (25), for a broad range of parameters.

Figure 13a shows time evolution of x and y obtained in numerical integration. The system generates a signal in the form of radio pulses following each other with the period of parameter modulation, but the phase of the high-frequency filling signal jumps chaotically between the pulses. Figure 13b plots the map for the phase taken at the middle of the excitation stage of the first oscillator, $\varphi = \arg(x_0 - \mathrm{i}x_1)$, pertaining to the dynamics on the attractor, as obtained in numerical simulations. It shows points $(\varphi_n, \varphi_{n+1})$ for a sufficiently large number of periods T. As follows from the figure, a single circle cycle for the preimage, i.e., variation of the variable φ_n from zero to 2π, corresponds to two cycles for the image φ_{n+1}.

For a more accurate description of the system dynamics in discrete time, the system state at the instant $t_n = nT$ is specified by four variables composing the vector $\mathbf{x}_n = \{x(nT), u(nT), y(nT), v(nT)\}$, where $u = \omega_0^{-1}\dot{x}$ and $v = \omega_0^{-1}\dot{y}$. The solution of Eqn (25) over the time interval T with initial conditions $\mathbf{x}_n$ provides the new vector $\mathbf{x}_{n+1}$, which corresponds to the four-dimensional Poincaré map

$$\mathbf{x}_{n+1} = \mathbf{T}(\mathbf{x}_n) . \tag{27}$$

From a geometrical standpoint, the flow of trajectories in the five-dimensional augmented phase space of the nonautonomous system $\{x, u, y, v, t\}$ is dissected with four-dimensional hypersurfaces $t = t_n = nT$.

According to the computation results, the Lyapunov exponents related to the Poincaré map for the selected parameters are

$$\Lambda_1 = 0.6832,\ \Lambda_2 = -2.602,\ \Lambda_3 = -4.605,\ \Lambda_4 = -6.538. \tag{28}$$

The positive exponent Λ_1, signaling the presence of chaos, is close to the value $\ln 2 = 0.693$, which is natural because of the approximate description of the evolution of the phase variable with one-dimensional map (26). The estimate of the attractor dimension provided by the Kaplan–Yorke formula is $D \approx 1.263$.

When map (27) is iterated in its four-dimensional space, dilation occurs in the direction associated with the phase featured by Eqn (26), and contraction occurs along the other three directions. The absorbing toroid-shaped domain U can be identified. One map iteration corresponds to the longitudinal dilation and transverse contraction of the object, which is then put in the form of a double loop inside the initial domain. This corresponds to the Smale–Williams construction, but in the four-dimensional space. Figure 13c depicts a three-dimensional projection of four-dimensional objects,

giving an idea of the mutual location of domains U and $\mathbf{T}(U)$. The domain $\mathbf{T}(U)$ looks like a narrow band because of the strong transverse contraction of the phase volume in the process of evolution over one period.

The diagrams in Fig. 13d display images of the system attractor. Shown in the left panel is the projection from the augmented five-dimensional space on the phase plane of the first oscillator in the variables (x, u). The attractor is visualized through shadows of gray (the density of color is defined by the relative frequency of visits of the representing point to the respective image pixel). The points related to the Poincaré section, i.e., to the instants $t_n = nT$, are plotted in black. The nearest panel shows the portrait of the attractor in the Poincaré section on the plane (x_0, x_1) that corresponds to the fragment inside the dashed parallelogram. There is an obvious visual similarity with the Smale–Williams attractor. The transverse Cantor structure of the attractor is illustrated in the right diagrams in Fig. 13d with the sequence of details with increased magnification. The hyperbolic nature of the attractor is confirmed by numerical computations based on the cone criterion [84, 85]. The hyperbolic nature of the attractor of model (25) was recently substantiated on the level of a computer-assisted proof [86], similar to the earlier proof for the quasihyperbolic attractor of the Lorentz system in the well-known work by Tucker [51].

Under the assumption that $N = \omega_0 T/2\pi \gg 1$, the problem can be reformulated with the help of the method of slowly varying complex amplitudes, which reduces the number of defining parameters. For this, we assume that $x = 2\,\mathrm{Re}\,a(t)\exp(\mathrm{i}\omega_0 t)$, $\dot{x} = -2\omega_0\,\mathrm{Im}\,a(t)\exp(\mathrm{i}\omega_0 t)$, $y = 2\,\mathrm{Re}\,b(t)\exp(2\mathrm{i}\omega_0 t)$, and $\dot{y} = -4\omega_0\,\mathrm{Im}\,b(t)\exp(2\mathrm{i}\omega_0 t)$. Inserting these in Eqns (25) and averaging over the period of fast oscillations gives

$$\dot{a} = \frac{1}{2}\left(aA\cos\frac{2\pi t}{T} - |a|^2 a - \mathrm{i}\bar{\varepsilon}b\right),$$

$$\dot{b} = \frac{1}{2}\left(-bA\cos\frac{2\pi t}{T} - |b|^2 b - \mathrm{i}\bar{\varepsilon}a^2\right), \qquad (29)$$

where $\bar{\varepsilon} = \varepsilon/2\omega_0$. System (29) is analyzed in Ref. [87]. It is shown there that the Smale–Williams attractor is realized in the Poincaré map for a broad range of parameters, which is confirmed by testing the cone criterion in numerical simulations, in particular, for $A = 3$, $T = 10$, and $\bar{\varepsilon} = 0.05$.

As already mentioned, system (25) is constructed such that the terms responsible for the coupling contain frequency components that are in resonance with the oscillator receiving the excitation. It is shown in [88] that the Smale–Williams attractor may occur in a system with alternately active oscillators, even for a nonresonant excitation transfer. Indeed because the characteristic excitation time of the partner oscillator is finite, the spectrum of the signal involved in the transfer of excitation occupies some band around its central frequency, with tails decaying on both sides. For example, if the central frequency is $2\omega_0$ and the frequency of the oscillator to be excited is ω_0, then, under certain conditions, the presence of the signal at the tail of the spectral distribution in the vicinity of the frequency ω_0 can facilitate the excitation transfer. Moreover, at the active stage, the growth of oscillations follows an exponential law if the bifurcation threshold is surpassed by a certain finite increment. Admittedly, the limitations on the parameters of the system become more stringent in this case.[13] According to the results of computations, in the system

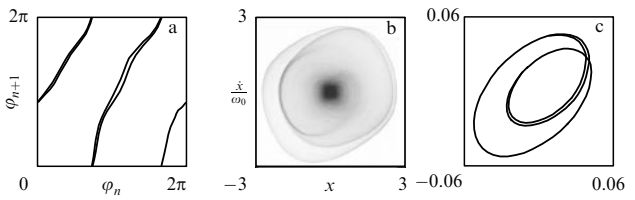

Figure 14. (a) Diagram for the phases defined as $\varphi = \arg(x - \mathrm{i}\dot{x}/\omega_0)$, the portrait of an attractor in the projection on the phase plane of the first oscillator (b) and in the Poincaré section (c) for the system of oscillators coupled through a nonresonance mechanism of excitation transfer, described by Eqns (30) for $T = 10$, $\omega_0 = 2\pi$, $\varepsilon = 0.5$, and $A = 6$.

$$\ddot{x} - \left(A\cos\frac{2\pi t}{T} - x^2\right)\dot{x} + \omega_0^2 x = \varepsilon y,$$

$$\ddot{y} - \left(-A\cos\frac{2\pi t}{T} - y^2\right)\dot{y} + 4\omega_0^2 y = \varepsilon x^2 \qquad (30)$$

for the set of parameters $T = 10$, $\omega_0 = 2\pi$, $\varepsilon = 0.5$, and $A = 6$, a Smale–Williams attractor can be observed in the Poincaré map, although the transfer of excitation from the second oscillator to the first bears a nonresonant character. Figure 14 shows a diagram for phases at subsequent stages of activity of the first oscillator, and also the image of the attractor in the projection from the augmented phase space on the plane $(x, \dot{x})$ and the portrait of the attractor in the Poincaré section. The Lyapunov exponents for the Poincaré map in this regime are $\Lambda_1 = 0.6808$, $\Lambda_2 = -3.625$, $\Lambda_3 = -8.326$, and $\Lambda_4 = -17.633$, while the estimate of the dimension with the Kaplan–Yorke formula gives $D_{\mathrm{KY}} = 1.188$.

9.2 The Smale–Williams attractor in an autonomous system

Several examples of autonomous systems featuring the Smale–Williams attractor in the Poincaré map were proposed in [89]. We consider one of them, which is interesting because its phase space dimension is just the minimum needed for the existence of such an attractor.

We begin with a modified system of the 'predator–prey' type:

$$\dot{r}_1 = 2\left(1 - r_2 + \frac{1}{2}r_1 - \frac{1}{50}r_1^2\right)r_1,\ \dot{r}_2 = 2(r_1 - 1)\,r_2\,. \qquad (31)$$

We regard the nonnegative variables $r_{1,2}$ as squared amplitudes of two oscillators and write the equations for the complex-valued amplitudes a_1 and a_2 such that the quantities $r_{1,2} = |a_{1,2}|^2$ exactly satisfy Eqns (31). We assume the frequency of oscillations to be specified by the parameter ω_0. Additionally, we introduce coupling between the oscillators by adding a term containing the square of the complex-valued amplitude a_2 to the equation for the first complex-valued amplitude, and a term with the first power of a_1 to the

[13] Apparently, the resonance mechanism should be considered the preferred one in relation to various physical applications (for example, in microwave electronics, laser physics, or nonlinear optics) because reaching a level in nonresonant excitation transfer above the noise background may appear problematic.

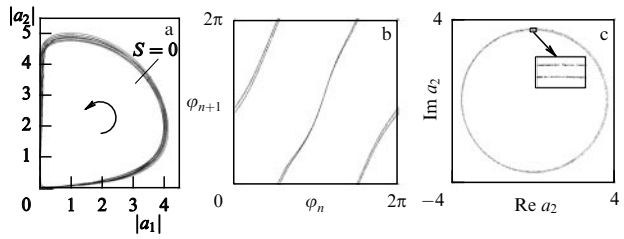

Figure 15. (a) Portrait of the attractor of system (32) in the projection on the plane of real-valued amplitudes $|a_1|$ and $|a_2|$. The interval of the bisectrix corresponds to the section used to construct the Poincaré map. (b) Map for the phase $\varphi = \arg a_2$ determined for the sequence of moments when a trajectory belonging to the attractor intersects the section surface. (c) Portrait of the attractor in a stroboscopic section. The parameters are $\omega_0 = 2\pi$ and $\varepsilon = 0.3$.

other equation.[14] We have

$$\begin{aligned}\dot{a}_1 &= -\mathrm{i}\omega_0 a_1 \\ &\quad + \left(1 - |a_2|^2 + \frac{1}{2}\,|a_1|^2 - \frac{1}{50}\,|a_1|^4\right) a_1 + \frac{1}{2}\,\varepsilon\,\mathrm{Im}\,a_2^2\,, \\ \dot{a}_2 &= -\mathrm{i}\omega_0 a_2 + \left(|a_1|^2 - 1\right) a_2 + \varepsilon\,\mathrm{Re}\,a_1\,.\end{aligned} \tag{32}$$

Figure 15a presents the image of an attractor in the projection on the plane of real-valued amplitudes of both oscillators for $\omega_0 = 2\pi$ and $\varepsilon = 0.3$.

The instantaneous system state is defined by two complex-valued quantities a_1 and a_2, and hence the phase space has dimension 4. We select the three-dimensional hypersurface $S = |a_2|^2 - |a_1|^2 = 0$ in the phase space and consider its intersection by trajectories in the direction of increasing S. A point in the section is defined by a three-dimensional vector, and we therefore have a three-dimensional Poincaré map.

In the stationary regime, as can be seen from the results of the numerical solution of the equations, in particular from Fig. 15a, the representing point repeatedly visits the vicinity of the origin in the plane of $|a_1|$ and $|a_2|$. Each such visit is followed first by the excitation of the first oscillator, then by the excitation of the second, then by the decay of oscillations of the first, and finally by a slower decay of the second. The activation of the second oscillator occurs because of the action from its partner, owing to the added term in the second equation; therefore, the second oscillator inherits the phase of the first. Then, in the decay phase, the second oscillator provides a seed signal for the first one when the orbit passes in the vicinity of the origin. Because the responsible term contains the square of the complex-valued amplitude, the excitation transfer is accompanied by phase doubling. (Here, a nonresonant mechanism occurs.) The process is repeated in time. In every new cycle, the phase is multiplied by 2 and the Bernoulli map should follow in a certain approximation.

Figure 15b plots the map for the phase, drawn using the results of a numerical solution of Eqns (32). The phase is determined at the instant the trajectory hits the section surface $S = 0$ as the argument of the complex-valued amplitude a_2. It can be seen from the figure that the desired topological property is observed: one single cycle over the circle for the preimage corresponds to two cycles for the image. Because the Poincaré map ensures contraction with respect to other directions, the Smale–Williams attractor obviously occurs in its three-dimensional space.

Figure 15c shows the portrait of the attractor in the Poincaré section in the projection on the phase plane of the second oscillator. The attractor has a fine transverse fractal structure, whose magnified detail is shown in the inset.

Computing Lyapunov exponents with the help of the Benettin algorithm for model (32) leads to the results

$$\lambda_1 = 0.0918,\ \lambda_2 = 0.0000,\ \lambda_3 = -0.982,\ \lambda_4 = -1.330. \tag{33}$$

Taking the autonomous nature of the system into account, it is natural to suppose that the exponent λ_2 is exactly zero. According to the results of numerical simulations, the mean period between the subsequent intersections of the Poincaré section is $\langle T\rangle = 7.248$. In accordance with the approximation based on the Bernoulli map, the largest Lyapunov exponent must then be $\ln 2/\langle T\rangle \approx 0.096$. This is in reasonable agreement with the value of λ_1 derived from numerical simulations. The estimate of the attractor dimension based on the Kaplan–Yorke formula gives $D_\mathrm{L} = 2 + (\lambda_1 + \lambda_2)/\lambda_3 \approx 2.094$. Numerical simulations were carried out for the system of equations (32) for the above values of the parameters. They confirmed that the cone criterion is valid in the toroidal domain containing the attractor of the Poincaré map [90].

In our recent work [66], we suggested how to modify system (32) such that it follows the scenario when the Smale–Williams attractor occurs through the blue sky catastrophe, in accordance with the theory of Shil'nikov and Turaev (see Section 6). For this, it is necessary to modify the structure of the nonlinear factor in the second equation and introduce a parameter μ such that the system becomes

$$\begin{aligned}\dot{a}_1 &= -\mathrm{i}\omega_0 a_1 + \left(1 - |a_2|^2 + \frac{1}{2}\,|a_1|^2 - \frac{1}{50}\,|a_1|^4\right) a_1 \\ &\quad + \frac{1}{2}\,\varepsilon\,\mathrm{Im}\,a_2^2\,, \\ \dot{a}_2 &= -\mathrm{i}\omega_0 a_2 + \left(|a_1|^2 - \mu + \frac{1}{2}|a_2|^2 - \frac{1}{50}|a_2|^4\right) a_2 + \varepsilon\,\mathrm{Re}\,a_1\,.\end{aligned} \tag{34}$$

For the parameters chosen for the detailed analysis, $\omega_0 = 2\pi$ and $\varepsilon = 0.5$, two limit cycles in the phase space, stable and unstable ones, are located in the domain where the amplitude of the first oscillator $|a_1|$ is small, as long as μ is less than the critical value $\mu_0 \approx 3.144196$. Figure 16a displays a transient trajectory approaching the stable limit cycle. As the parameter μ increases, the limit cycles approach each other, coalesce at $\mu = \mu_0$, and disappear. After that, the attractor is formed by the set of trajectories that concentrate at the location of the pair of limit cycles that have just disappeared, such that the trajectories belonging to it repeatedly go into the vicinity of the origin (Fig. 16b). After the bifurcation, the dynamics consist of the excitation of the first oscillator followed by the other, the decay of the oscillations of the first oscillator, and the slower decay of the other, repeating in sequence. Over the full cycle of the excitation transfer between the oscillators, the phase is doubled. This corresponds to the index $m = 2$ in the theory of Shil'nikov and Turaev, and, consequently, to the birth of the Smale–Williams attractor in the Poincaré section. This is illustrated by the plot of the map for the phase based on the results of a numerical solution of the equations (Fig. 16c). The

[14] The particular choice of the form of these terms allows some ambiguity. Here, they are specified so as to maintain correspondence with the form of equations adopted in Ref. [89].

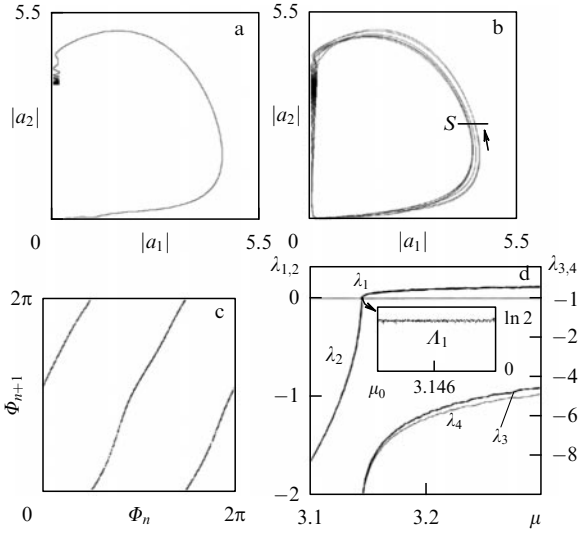

Figure 16. (a) Transient trajectory in the system of coupled oscillators (34) for $\mu = 3.14$ and (b) the portrait of the attractor at $\mu = 3.1442$ in the projection on the plane of amplitudes $|a_1|$ and $|a_2|$. (c) Diagram for phases of the first oscillator measured at the instants when the Poincaré section is crossed for $\mu = 3.1442$. (d) The dependence of the Lyapunov exponents of system (34) on the parameter μ. The inset in panel (d) shows the plot for the largest exponent of Poincaré map $\Lambda_1 = \lambda_1\langle T\rangle$. The other parameters are $\omega_0 = 2\pi$ and $\varepsilon = 0.5$.

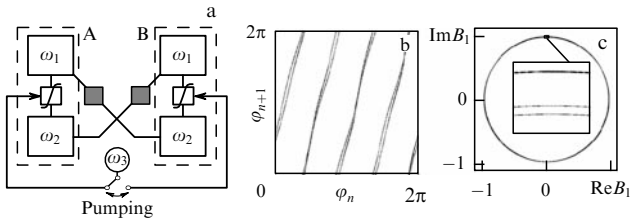

Figure 17. Schematics of a parametric chaos generator. Blocks labeled ω_1 and ω_2 are oscillators with the respective frequencies; the squares crossed with wavy lines are the reactive coupling elements characterized by a parameter oscillating with the pumping frequency ω_3; the dark squares are the elements of coupling with a quadratic nonlinearity. (b) Iteration diagram for the phase on the activity stage of one of the subsystems and (c) the portrait of the attractor in the Poincaré section in a projection on the plane of the complex-valued variable corresponding to the amplitude of the first oscillator in the second subsystem, based on the numerical solution of Eqns (35) with $\varkappa = 1.393$, $\varepsilon = 0.08$, $\alpha = 0.6$, $\beta = 1.184$, and $T = 40$.

phase is determined as $\Phi_n = \arg a_1(t_n)$ at the instant the trajectory intersects the section surface $|a_2| = 2.5$ in the direction of increasing $|a_2|$.

Figure 16d plots the Lyapunov exponents as a function of the parameter μ in the interval that includes the bifurcation point. In the left part of the plot, the largest exponent is equal to zero, and the other three are negative. Here, the stable limit cycle serves as an attractor, as in Fig. 16a. At the instant of bifurcation, two exponents vanish. After the bifurcation, one of them becomes positive and increases as μ increases. The second exponent stays equal to zero. The third and fourth exponents are negative. It can be verified that the positive exponent increases because of the reduction in the time the beam of trajectories performs a cycle, which behaves as $\langle T\rangle \sim (\mu - \mu_c)^{-1/2}$. The Lyapunov exponent for the Poincaré map $\Lambda_1 = \lambda_1\langle T\rangle$ stays nearly constant and is close to ln2 (see the inset in Fig. 16d), which agrees with the approximate description of phase transformations by the Bernoulli map.

9.3 Parametric generator of chaos

From the standpoint of applying the principle of manipulating the phase in the process of excitation transfer between partial oscillators, the class of systems with parametric excitation seems to be a proper choice [91–93]. Systems of this kind can be built on various physical bases — in electronics, mechanics, acoustics, or nonlinear optics.

One widely used scheme of parametric generation involves two oscillators that are coupled through a reactive (dissipationless) element governed by a parameter varying in time. The frequencies ω_1 and ω_2 of the oscillators and the frequency ω_3 of parameter variation, or the pumping frequency, are related as $\omega_1 + \omega_2 = \omega_3$, which expresses the condition of parametric resonance. Oscillations are generated simultaneously in both partial oscillators. Their amplitudes can be stabilized by adding a nonlinear resistive element to the scheme.

We consider a system [94] composed of two such subsystems, A and B (Fig. 17). Let the frequencies be chosen such that $\omega_2 = 2\omega_1$ and $\omega_3 = 3\omega_1$ (the parametric resonance condition is obviously satisfied). The oscillator with the frequency ω_1 available in each subsystem is assumed to be coupled via a quadratic nonlinear element to the oscillator having the frequency ω_2 of the partner subsystem. By virtue of the frequency selection, the effect of one oscillator on the other is resonant on the second harmonic.

Let the pumping be switched on alternately in both subsystems, such that the functioning of the setup consists in alternating parametric excitation of the subsystems with a subsequent decay in time intervals between the active stages. At the beginning of a successive excitation stage in each of the subsystems, the developing oscillations are triggered by the signal from the partner subsystem on the second harmonic. The excitation transfer is therefore each time accompanied by the doubling of the oscillation phase. Over the full period of pumping modulation, the oscillation phase is multiplied by 4, which ensures chaos in the behavior of the sequence of phase values. The system generates a signal in the form of pulses following each other with the period of the pumping modulation, while the phase of high-frequency filling jumps chaotically from pulse to pulse.

Following the standard approach for parametric systems, we turn to the description in terms of slowly varying amplitudes [91–93]. We let the complex-valued amplitudes of two oscillators of the first subsystem be denoted by A_1 and A_2, and those of the second by B_1 and B_2. Taking the relation between frequencies into account, we write the equations

$$\begin{aligned}
\dot{A}_1 &= -\varkappa f(t)\, A_2^* - \mathrm{i}\varepsilon A_1^* B_2 - \frac{1}{2}\,\alpha A_1 - \frac{1}{2}\,\beta A_1 |A_1|^2,\\
\dot{A}_2 &= -\frac{1}{2}\,\varkappa f(t)\, A_1^* - \frac{1}{4}\,\mathrm{i}\varepsilon B_1^2 - \frac{1}{2}\,\alpha A_2 - 2\beta A_2 |A_2|^2,\\
\dot{B}_1 &= -\varkappa g(t)\, B_2^* - \mathrm{i}\varepsilon B_1^* A_2 - \frac{1}{2}\,\alpha B_1 - \frac{1}{2}\,\beta B_1 |B_1|^2,\\
\dot{B}_2 &= -\frac{1}{2}\,\varkappa g(t)\, B_1^* - \frac{1}{4}\,\mathrm{i}\varepsilon A_1^2 - \frac{1}{2}\,\alpha B_2 - 2\beta B_2 |B_2|^2.
\end{aligned} \tag{35}$$

The parameter ε controls the nonlinear coupling between the oscillators belonging to different pairs. The coefficients α and β respectively characterize the linear and nonlinear dissipa-

tion. The parameter $\varkappa$ determines the intensity of pumping at the frequency $\omega_3 = \omega_1 + \omega_2 = 3\omega_1$, and the functions $f(t)$ and $g(t)$ determine the slow dependence of the pumping amplitude on time in the two subsystems; we assume that

$$f(t) = \sin^2 \frac{\pi t}{T}, \quad g(t) = \cos^2 \frac{\pi t}{T}. \tag{36}$$

Figure 17b shows the diagram for phases that correspond to subsequent stages of excitation of the second system, $\varphi_n = \arg B_1(nT)$, constructed on the basis of numerical integration of Eqns (35). (We emphasize that the phase pertains to the active stage of the subsystem in question, when its amplitude is certainly different from zero.) We note that a single circle cycle for the preimage, i.e., the variation of the phase φ_n from zero to 2π, corresponds to four circles for the image φ_{n+1}. This implies that the map for the phase is identified with the same topological class as the dilating map of the circle $\varphi_{\text{new}} = 4\varphi_{\text{old}}$.

Figure 17c shows the phase portrait of the attractor in the Poincaré section in a projection on the plane of dynamical variables of the first oscillator of the second subsystem. The inset magnifies the details of the fine transverse fractal structure of the attractor. The full spectrum of Lyapunov exponents for the attractor is

$$\lambda_1 = 0.03456,\ \lambda_2 = -0.1320,\ \lambda_3 = -0.2247,$$
$$\lambda_4 = -0.5220,\ \lambda_5 = -0.6826,\ \lambda_6 = -0.9012,$$
$$\lambda_7 = -1.419,\ \lambda_8 = -2.325. \tag{37}$$

The presence of the positive exponent λ_1 quantitatively confirms the existence of chaos. The other exponents are negative. It then follows that an element of phase space experiences dilation along a single direction and contraction along all other directions in the phase space of the Poincarée map. For the Poincaré map, the Lyapunov exponents are related to those in (37) as $\Lambda_k = \lambda_k T$. Hence, $\Lambda_1 = 1.382$, which agrees well with the value $\ln 4 = 1.3862\ldots$, which corresponds to an approximate description of the phase variable evolution governed by the Bernoulli map.

The estimate of the attractor fractal dimension based on Lyapunov exponents (37) and the Kaplan–Yorke formula gives $D = 1 + \Lambda_1/|\Lambda_2| \approx 1.26$ for the attractor in the Poincaré map (because $\Lambda_1 > 0$ and $\Lambda_1 + \Lambda_2 < 0$). Correspondingly, for the attractor of the original system embedded into the augmented 9-dimensional phase space, the dimension becomes $D' = D + 1 \approx 2.26$.

The nature of the mechanism underlying the system functioning, as well as the numerical results confirming its realization, provide rationale to conjecture that the observed attractor is uniformly hyperbolic. Interpreting the action of the Poincaré map geometrically, we can imagine a toroid (a direct product of a one-dimensional circle and a seven-dimensional sphere) embedded into an eight-dimensional space and relate a single iteration of the map with longitudinal dilation and transverse contraction of this object, which is then embedded into the original domain as a four-fold loop. At each step of this procedure, the number of loops increases four times. In the limit, we obtain an attractor with an infinite number of loops — a variant of the Smale–Williams solenoid. Although the conjecture on the uniformly hyperbolic nature of the attractor is in this case hypothetical, the system considered here can be interesting in and of itself because it offers the possibility of generating chaotic regimes that are insensitive to the choice of parameters and characteristics of the element in systems pertaining to radio engineering and electronics, acoustics, and nonlinear optics.[15]

10. The possibility of implementing a Smale–Williams-type attractor in systems with delay

To implement the principle of phase manipulation in the excitation transfer, we can consider systems with a delay [96–98] as an alternative to systems based on oscillators excited one after another. In this case, it suffices to have a single oscillator that alternately stays in active or decaying regimes, while the transfer of excitation between the stages, with an appropriate phase transformation, is carried through the delaying feedback circuit. From the standpoint of practical realization, such systems can even be simpler than the alternately excited oscillators. From the mathematical standpoint, they are more complex because the presence of delay formally implies that their state space is infinite dimensional. An accurate mathematical analysis of attractors in such systems, including rigorous verification of the hyperbolicity hypothesis, constitutes a difficult problem calling for the development of new approaches.

We consider a model system described by the equation [96]

$$\ddot{x} - \left(A\cos\frac{2\pi t}{T} - x^2\right)\dot{x} + \omega_0^2 x = \varepsilon x(t-\tau)\,\dot{x}(t-\tau)\cos\omega_0 t\,. \tag{38}$$

Here, x is the dynamical variable of the van der Pol oscillator with the working frequency ω_0, in which the parameter controlling the bifurcation of the limit cycle birth slowly varies in time with the period T and amplitude A, such that the oscillator stays alternately in the regimes of excitation and decay of oscillations. A term responsible for a delayed feedback is added to the right-hand side of (38). It is given by the product of the dynamical variable reduced by the time interval τ, its derivative, and an auxiliary signal at the frequency ω_0. The parameter ε determines the magnitude of the delaying feedback. We assume that $N = \omega_0 T/2\pi$ is an integer, such that the external action on the system, including the parameter modulation and auxiliary signal, is periodic.

The functioning of system (38) as a chaos generator can be explained as follows. Owing to the periodic variation in the parameter responsible for the onset of generation, the oscillator is found in alternating regimes of excitation and decay of oscillations. With an appropriate choice of the time lag, for example, $\tau = (3/4)\,T$, we can create a situation where at each activity stage, the seed for the developing self-sustained oscillations is provided by the signal generated during the previous activity stage. We suppose that the signal has a certain phase φ, i.e., $x(t) \sim \sin(\omega_0 t + \varphi)$ and $\dot{x}(t) \sim \cos(\omega_0 t + \varphi)$. Then the term in the right-hand side of Eqn (38) contains a component at the basic frequency ω_0 with

[15] An example of a parametric chaotic generator comprising two coupled oscillators with nonlinear dissipation and modulation of their Q-factors was recently proposed in [94]. The dynamics are described by a non-autonomous system of fourth-order equations. The presence of the Smale–Williams attractor is shown for a four-dimensional Poincaré map. Additionally, the computer-assisted test of the cone criterion is undertaken, confirming the hyperbolic nature of the attractor.

the doubled phase. Indeed,

$$x(t-\tau)\,\dot{x}(t-\tau)\cos\omega_0 t \sim \sin 2\big[\omega_0(t-\tau)+\varphi\big]\cos\omega_0 t$$
$$= \frac{1}{2}\sin(\omega_0 t - 2\omega_0\tau + 2\varphi) + \ldots, \qquad (39)$$

where the dots denote nonresonant terms. Therefore, at the new activity stage, the phase of oscillations its defined by that of the resonant component of the seed signal, and at subsequent stages of activity, we obtain the Bernoulli map $\varphi_{n+1} = 2\varphi_n + \text{const} \pmod{2\pi}$. If the phase volume is contracted along all other directions of the state space, the dynamics of this kind should correspond to the presence of the Smale–Williams attractor for the map of the phase space into itself over the period of external action.

Figure 18a plots the oscillations obtained by numerical integration of Eqn (38), which corresponds to the motion on the attractor. The chaos is manifested through the random position of filling oscillations with respect to the envelope at subsequent activity stages. Figure 18b presents the diagram for phases determined at subsequent activity stages, showing the agreement with the doubly dilating map of a circle. Figures 18c and d show the portrait of the system attractor in a projection from the infinite-dimensional state space on the oscillator phase plane $(x,\ \dot{x})$, and the portrait of the attractor in the Poincaré section. The transverse fractal structure can be distinguished in the second image. It is a characteristic feature of the Smale–Williams attractor.

Speaking formally, the attractor has an infinite number of Lyapunov exponents because of the infinite-dimensional nature of a system with delay. From a practical standpoint, it is sensible to limit ourself to considering a finite subset of them, namely, the exponents that are largest in magnitude, whose number suffices for determining the dimension according to the Kaplan–Yorke formula. Computations based on the Benettin algorithm, adapted to systems with delay, lead to the following values of the exponents over the period T for the chosen values of parameters:

$$\Lambda_1 = 0.688,\ \Lambda_2 = -0.837,\ \Lambda_3 = -4.287. \qquad (40)$$

The only positive exponent of the attractor is numerically close to $\ln 2 = 0.693\ldots$, which agrees with the approximation

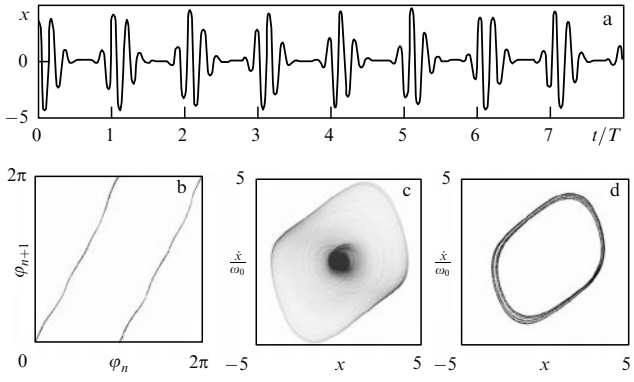

Figure 18. (a) Time dependence of the dynamical variable according to numerical solution of Eqn (38). (b) Diagram illustrating the phase transformation at sequential stages of the oscillator activity, found by solving Eqn (38) numerically at $\omega_0 = 2\pi$, $T = 6$, $\tau = 3/4T$, $A = 5.5$, and $\varepsilon = 0.2$. The portrait of the attractor of system (38) in a projection from the infinite-dimensional state space on the oscillator phase plane $(x, \dot{x})$ (c), and the portrait of the attractor in the Poincaré section (d).

that resorts to the description of phase dynamics through the Bernoulli map. The estimate of the dimension by the Kaplan–Yorke formula gives $D_{KY} = 1 + \Lambda_1/|\Lambda_2| \approx 1.82$ for the map over the period. The dimension of the attractor as an object in the augmented phase space is larger by one.

The mechanism of model functioning and numerical results confirming its realization suggest the assumption that the observed chaotic attractor is uniformly hyperbolic, or more specifically is a Smale–Williams-type attractor embedded into the infinite-dimensional state space of the system with delay. Despite the hypothetical character of this conjecture, the scheme of the chaos generator considered above may have an independent interest because it offers a framework for obtaining chaotic regimes insensitive to the choice of parameters and constructive details in systems of radio engineering and electronics, nonlinear optics, and other areas.

Two more models of nonautonomous systems with delay, exploiting the idea of phase manipulation for the generation of chaotic dynamics, are considered in Refs [97, 98]. In contrast to system (38), the presence of two delayed feedback chains enables the resonance mechanism of transferring excitation from the preceding stages of oscillator activity without resorting to an auxiliary signal with the frequency ω_0. It is supposed that attractors of these systems fit into the class of *partly hyperbolic* [20, 26], because of a neutral direction associated with a Lyapunov exponent that is close to zero.

11. Realization of hyperbolic attractors in electronic devices

As stated in the Introduction, the development of a physical approach to hyperbolic attractors should result in the design of functioning generators of chaos. Two examples of electronic devices implemented thus far as laboratory setups [99, 96] are considered below. A variant of the scheme of a hyperbolic chaos generator in the microwave band based on coupled drift klystrons, described in Ref. [100], can also be mentioned alongside them.

11.1 Scheme based on coupled self-oscillators with alternating excitation

Figure 19 shows the schematic of a device representing a nonautonomous oscillatory system composed of two subsystems, the van der Pol oscillators [99]. Each oscillator contains a tuned circuit composed of a coil with inductance $L_{1,2}$ and a capacitor with capacitance $C_{1,2}$, such that $\omega_0 = 1/\sqrt{L_1 C_1}$, $2\omega_0 = 1/\sqrt{L_2 C_2}$. The negative resistance is provided by a special element based on an operational amplifier. The nonlinear conductivity that assures an increase in energy loss with an increase in the oscillation amplitude is introduced by an element composed of semiconductor diodes ($D_1 - D_6$, $D_7 - D_{12}$), made of two branches transmitting electric current in opposite directions and connected in parallel. The field-effect transistor ($T_{1,2}$) introduces a practically linear positive conductivity in the circuit, whose magnitude is controlled by the voltage applied to the gate of the transistor, which slowly varies in time, performing oscillations with the period $T = 2\pi N/\omega_0$, where N is an integer. During half the period of this process, the first oscillator is in the regime of oscillation generation, and the second stays below the generation threshold, and vice versa during the other half. The first oscillator acts on the second

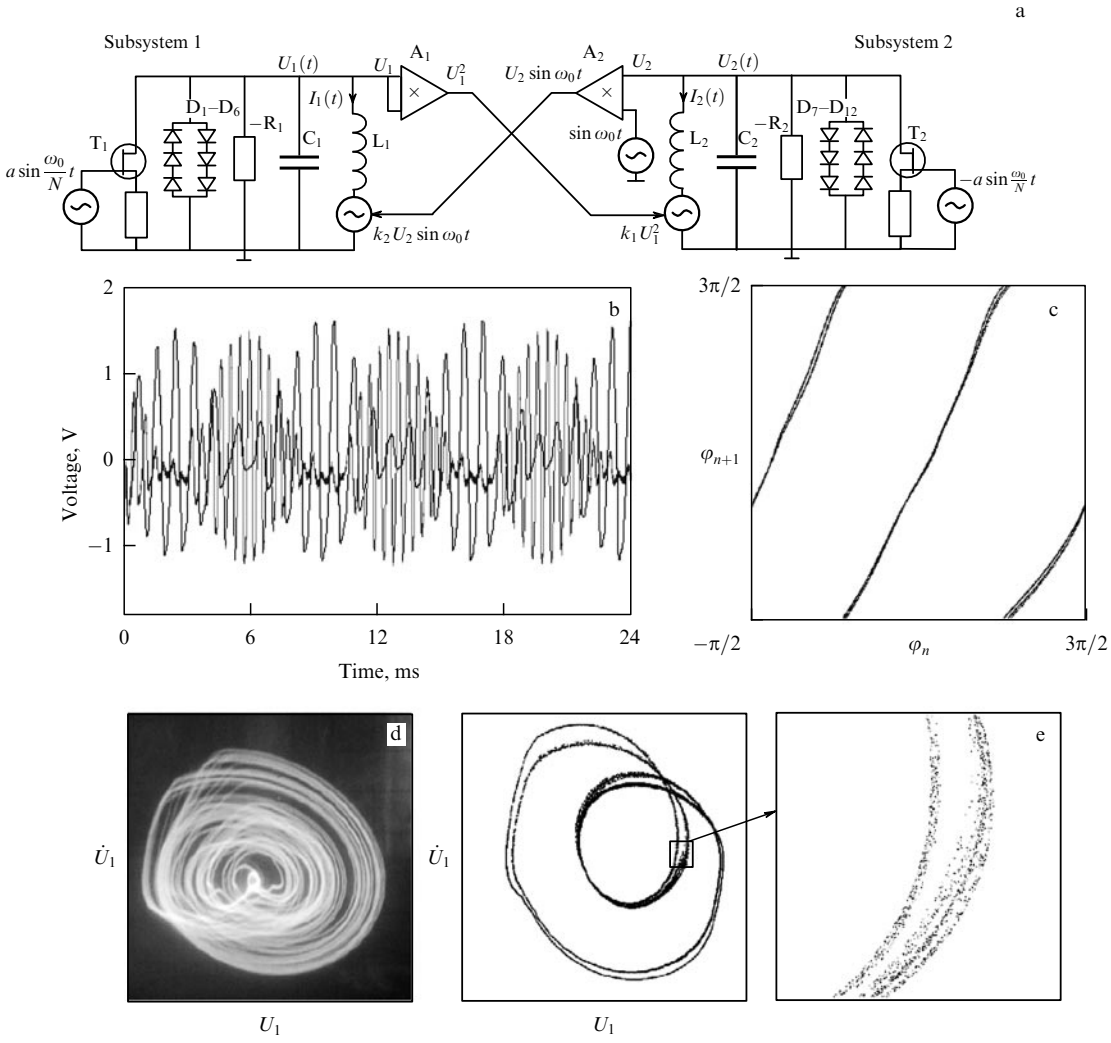

Figure 19. Schematics of a setup based on two coupled subsystems, van der Pol oscillators with periodically varying parameters. (b) Typical realizations of the time series of alternating voltage for the first (dark color) and second (light color) subsystems obtained in experiment with $N = 8$. (c) Iteration diagram for the phase of the first subsystem for $N = 8$. (d) Photo taken from the oscilloscope screen of the attractor portrait in a projection on the plane of the dynamical variables of the first oscillator $(U_1, \dot{U}_1)$ for $N = 4$. (e) Stroboscopic section of this attractor for the sequence of time instants separated by a period T in time and corresponding to the maximum of the first oscillator amplitude.

one via the nonlinear quadratic element A_1. In turn, the second oscillator acts on the first one via the nonlinear quadratic element A_2 that mixes the incoming signal with an auxiliary signal of the frequency ω_0. The functioning of the system corresponds to the idea outlined at the beginning of Section 9.1, and Eqns (25) can serve as a model, at least on a qualitative level of analysis.

In the laboratory setup implementation, the capacitors had the capacitance $C_1 = 20$ nF and $C_2 = 5$ nF, and the coil inductances L_1 and L_2 were about 1 H. The working frequencies of the oscillators were $f_1 = \omega_0/2\pi = 1090$ Hz and $f_2 = 2f_1 = 2180$ Hz. The output voltage U_1 and U_2 from the first and second circuits could be fed to recording devices (an oscilloscope or spectral analyzer) or registered with a computer as a time series with the help of an analog-to-digital converter. The functions $\dot{U}_1$ and $\dot{U}_2$ were obtained by analog differentiation with the use of a standard differentiating circuit containing a capacitor, resistor, and operational amplifier.

With the properly selected parameters in the system, chaotic oscillations ensuing from alternating stays of the oscillators in active regimes and the transfer of excitation from one oscillator to another with the corresponding phase transformation can be observed. Figure 19b shows the time dependences of the variable voltage in the regime of chaotic generation in both subsystems when the ratio of the frequencies of slow parameter variation and the auxiliary signal is $N = 8$. Plotting them was computer assisted and based on time series stored in memory. These were obtained through digitizing the voltage $U_1(t)$ and $U_2(t)$. The sampling frequency was 200 kHz, i.e., one period of the characteristic generation frequency ω_0 was covered with approximately 200 readings. Figure 19c depicts an iterative diagram for phases obtained experimentally by computer-aided processing of a two-component time series. One component corresponds to the sampled signal U_1 with the period of slow parameter variation $T = 2\pi N/\omega_0$ at time instants when the first oscillator amplitude attained a maximum. The second component was given by the derivative at the output of the differentiating circuit at the same instants. The phase was determined from the formula $\varphi = \arg(U_1 - i\omega_0^{-1}\dot{U}_1)$. The horizontal and vertical axes in the diagram correspond to the values of phase at successive instants of sampling. The fact that the phase map is topologically equivalent to a dilating

circle map should be considered a confirmation that the realized attractor has the nature of a Smale–Williams solenoid.

Figure 19d displays a photo of the phase portrait of an attractor in the chaos generation regime, taken from an oscilloscope screen. The inputs for the horizontal and vertical ray deflection were respectively fed with alternating voltage from the first subsystem $U_1(t)$ and the output signal of the differentiating circuit, which is proportional to $\dot{U}_1(t)$. Figure 19e shows the portrait of the attractor in a stroboscopic section projected on the plane $(U_1,\ \dot{U}_1)$, built by processing the two-component time series corresponding to the image of the Smale–Williams solenoid. The largest Lyapunov exponent, assessed by processing the time series using the technique in Ref. [101] with the sampling period T, is $\Lambda \approx 0.73$, which is in agreement with the estimate $\Lambda \approx \ln 2$ based on the Bernoulli map. The spectrum of oscillations is continuous for both oscillators: it spans a range near the frequency ω_0 for the first oscillator and near $2\omega_0$ for the second.

Unfortunately, not all theoretical results discussed in Section 9 can be tested experimentally. For example, it is difficult to assess the full spectrum of the Lyapunov exponents or to test the hyperbolicity by applying the cone criterion. Nevertheless, bearing in mind the totality of the results obtained, we can argue with a high degree of certainty that the experiment deals with the same object as is considered in the theoretical analysis, i.e., that the suspension of a Smale–Williams attractor is realized in the nonautonomous oscillatory system.

11.2 Scheme based on self-oscillators with delayed feedback

The schematic of an electronic device with delayed feedback, which implements the principle considered in Section 10, is shown in Fig. 20a [96]. The self-oscillator described approximately by the van der Pol equation contains an LC contour, an element with negative resistance based on the amplifier DA1, and a nonlinear dissipative element composed of diodes D1–D6. The principal oscillation frequency in the laboratory setup, $f = \omega_0/2\pi$, was 3 kHz.

The parameter controlling the excitation of self-oscillations is modulated by means of additional dissipation provided by the circuit on the field-effect transistor VT1 controlled by the external signal $A\cos(2\pi t/T)$. The period is $T \approx 6/f$; the oscillator stays in the generation regime during one half of the period and is below the generation threshold during the second half. The excitation of oscillations with a certain phase at the subsequent generation stage is ensured by the arrival of the delayed feedback circuit signal from the exit of multiplier DA3. In the feedback circuit, the signal undergoes a quadratic transformation (multiplier DA2) and differentiation by the standard differentiating circuit on elements R_1, C1, and DA4. The signal then passes through a digital delayed circuit that provides the time delay $3T/4$. As a result of multiplication with an auxiliary signal at the frequency ω_0, we obtain a signal with a frequency close to that of self-oscillations and the phase doubled relative to that at the instant t. This signal serves as a seed for the oscillator, stimulating its excitation at the next activity stage.

The signal generated by a functioning setup (see the oscillogram in Fig. 20b) was stored in digitized form with the help of an analog-to-digital converter as a time series, and was then used to construct the signal phase map for the period

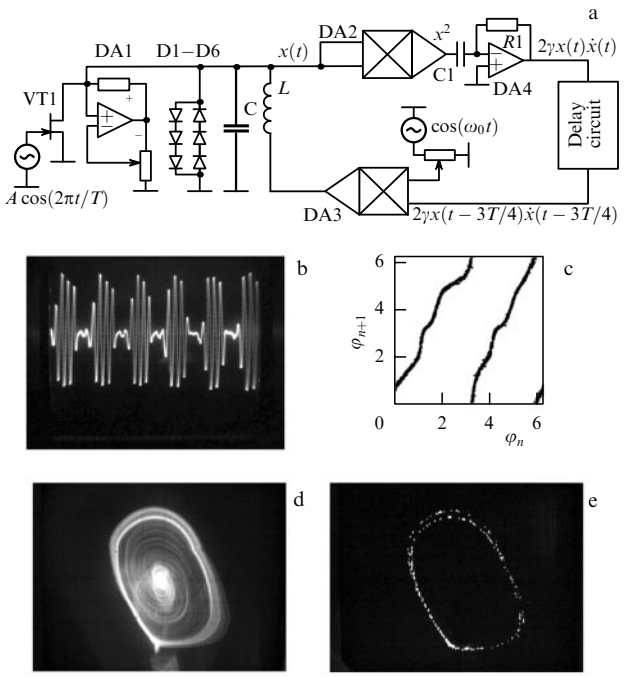

Figure 20. (a) Schematics of a hyperbolic chaos generator with a delayed feedback. (b) Time series of voltage across the capacitor C. (c) The iteration diagram for the phases of sequential trains of oscillations in the regime of chaos generation. (d) Projection of the phase portrait of the attractor and (e) its stroboscopic image.

T (Fig. 20c). As can be seen, the map obtained in this way belongs to the same topological class as the Bernoulli map, which is indicative of the presence of the Smale–Williams attractor. Figure 20d shows the portrait of the attractor projected on the oscillator phase plane taken as a screenshot from the oscilloscope. A stroboscopic map of the attractor in Fig. 20e demonstrates an obvious visual similarity with the Smale–Williams solenoid.

12. Conclusions

The material presented above is indicative of significant progress in the main areas of the research program sketched in the Introduction. It can be asserted that we now indeed have particular examples of physically realizable systems with chaotic dynamics to which the principles of hyperbolic theory are applicable (systems with axiom A).

Several ways of designing systems with uniformly hyperbolic attractors are identified: using models with pulse forcing; constructing dynamics as a set of stages replacing each other in succession; and constructing systems from oscillators that are excited alternately and prime each other subject to the phase transformation described by a map with chaotic dynamics. It is demonstrated how the principle of parametric excitation and a delayed feedback can assist the implementation of the hyperbolic chaos.

A set of particular systems is presented for which the presence of a uniformly hyperbolic attractor is confirmed by means of a computer-assisted test of the cone criterion or is anticipated based on qualitative arguments. The majority of systems considered here fall into the class of nonautonomous systems featuring time-periodic dependence of parameters or functions entering their equations. But there also exist examples of autonomous systems with the Smale–Williams

type of attractor in the Poincaré map. Owing to the structural stability property, these models admit certain modifications without losing the hyperbolic character of their dynamics, which allows designing new systems with uniformly hyperbolic chaos. Based on some of the proposed schemes, radioelectronic setups have been implemented, enabling demonstration of the dynamics on a hyperbolic attractor in experiment.

But the present discussion is limited to chaotic attractors in artificial systems constructed in a goal-oriented way, and not in systems of natural origin (where they are encountered rarely, if at all). The line between the two is not rigorously defined, of course. It should be kept in mind that the van der Pol oscillator acknowledged currently as a universal model in the theory of self-oscillations was initially applied only in an artificial technical system, the vacuum tube generator. Likewise, it can be hoped that models with hyperbolic attractors will eventually find their area of application in systems of natural origin, for example, in neurodynamics. The above-mentioned study by Belykh and coauthors [59] discussed the feasibility of a Plykin attractor in the Hindmarsh–Rose model of the neuron. In the same context, neurodynamics models with the blue sky catastrophe were considered in Ref. [64]. In that framework, situations corresponding to the presence of a Smale–Williams attractor can occur for the space dimension four or higher.

The possibility of the physical realization of hyperbolic chaos opens horizons for applications of a well-developed mathematical theory and paves the way for comparative studies of hyperbolic and nonhyperbolic chaos, including computer-assisted research and experiment. Also interesting and rich in content is the research area aimed at designing complex systems — chains, lattices, and networks composed of elements with hyperbolic chaos [102–104]. Presumably, the models constructed with the goal of realizing hyperbolic chaos will be useful in elucidating fundamental questions still challenging the research community, such as the problem of turbulence.

The question of diagnosing hyperbolic chaos in physical experiments is interesting in and of itself. Although mathematical techniques like the cone criterion seem less relevant in this perspective, the problem does not look insurmountable. At least in the case of the Smale–Williams attractor, the construction of an iteration diagram for phases, which demonstrates the correspondence with a dilating circle map, offers a productive and convincing way of uncovering the respective dynamics. This pertains to both computer simulations and experiment.

Over the last 20 years, active research on applications of chaotic signals in information–communication systems [105–108] has ben carried out. Although arguments in favor of this direction look convincing (larger information capacity of signals, the possibility of controlling dynamics through small perturbations, the diversity of ways the information can be embedded in the signal, and rich possibilities of encrypting for secure information transfer), it should also be acknowledged that the expected advantages are not realized to the full extent. A possible reason is that using signals generated by nonhyperbolic attractors does not allow relying on detailed theoretical explanations of the corresponding dynamics. On the other hand, the hyperbolic attractors benefit from the existence of a full, in a certain sense, mathematical description of chaos. For example, a complete listing of all trajectories belonging to an attractor is possible by associating them with sequences of symbols of a finite alphabet. It is therefore highly probable that the realization of the advantages promised by information–communication systems based on chaotic signals will see more progress when incorporating the hyperbolic chaos.

Systems employing the principle of phase manipulation [66, 78, 79, 87–89, 94–100] may be of special interest for schemes of secure communication. Chaos is manifested in this case in the irregular behavior of the phase in the generated sequence of radio pulses. This invites implementation of approaches that would ensure that the signal transfer in a communication channel is much less susceptible to noise, losses, and distortions than in the variants proposed thus far [105–108]. (In this respect, we recall the advantages of frequency and phase modulation over amplitude modulation known in traditional radio engineering.)

When discussing possible technological applications of systems with hyperbolic attractors, special attention should be paid to their most important properties such as structural stability or roughness.

The recent literature offers a broad discussion focused on the problem of so-called robust chaos [109–11]. This involves the dynamics such that no 'periodicity windows' emerge as the parameters are varied, while the dependence of the largest Lyapunov exponent is a smooth function over a wide parameter range. We stress that just such chaos is desirable for applications, in particular, for communication systems, random-number generators, or systems of information encoding. To obtain chaos of this type, it is proposed to use systems including elements with characteristics expressed in terms of functions with discontinuous derivatives. In practice, ideal slope breaks cannot be achieved, and hence fully excluding periodicity windows in this fashion seems problematic. In contrast, these properties of chaos emerge as natural attributes in systems with uniformly hyperbolic attractors because of the inherent structural stability.

The author is indebted for the fruitful discussions, help, and constructive criticism to V C Anishchenko, V S Afraimovich, B P Bezruchko, V N Belykh, A Yu Zhalnin, A Yu Zhirov, O B Isaeva, A P Kuznetsov, P V Kuptsov, J Kurths, R MacKay, A S Pikovsky, V I Ponomarenko, N M Ryskin, I R Sataev, E P Seleznev, V Tucker, D V Treshchev, D I Trubetskov, and L V Tyuryukina. This paper was supported in part by the grants RFBR 09-02-00426 and RFBR-DFG 08-02-91963, and the program "Development the Scientific Potential of High Schools" No 2.1.1/1738.

References

1. Sinai Ya G, Shil'nikov L P (Eds) *Strannye Attraktory* (Strange Attractors) (Moscow: Mir, 1981)
2. Hasselblatt B, Young L S, in *Encyclopedia of Nonlinear Science* (Ed. A Scott) (New York: Routledge, 2005) p. 11
3. Zaslavsky G M, Sagdeev R Z *Vvedenie v Nelineinuyu Fiziku: ot Mayatnika do Turbulentnosti i Khaosa* (Moscow: Nauka, 1988); Sagdeev R Z, Usikov D A, Zaslavsky G M *Nonlinear Physics: from the Pendilum to Turbulence and Chaos* (Chur: Harwood Acad. Publ., 1988)
4. Neimark Yu I, Landa P S *Stokhasticheskie i Khaoticheskie Kolebaniya* (Stochastic and Chaotic Oscillations) (Moscow: Nauka, 1988) [Transladed into English (Dordrecht: Kluwer Acad. Publ., 1992)]
5. Rabinovich M I, Trubetskov D I *Vvedenie v Teoriyu Kolebanii i Voln* (Oscillations and Waves in Linear and Nonlinear Systems) (Moscow-Izhevsk: RKhD, Inst. Komp'yut. Issled., 2000) [Rabinovich M I, Trubetskov D I (Dordrecht: Kluwer Acad. Publ., 1989)

6. Schuster H G, Just W *Deterministic Chaos*: *an Introduction* (Weincheim: Wiley-VCH, 2005) [Translated into Russian (Moscow: Mir, 1988)]
7. Thompson J M T, Stewart H B *Nonlinear Dynamics and Chaos* (Chichester: Wiley, 1986)
8. Dmitriev A S, Kislov V Ya *Stokhasticheskie Kolebaniya v Radiofizike i Elektronike* (Stochastic Oscillations in Radiophysics and Electronics) (Moscow: Nauka, 1989)
9. Loskutov A Yu, Mikhailov A S *Osnovy Teorii Slozhnykh Sistem* (Fundamentals of the Complex System Theory) (Moscow-Izhevsk: RKhD, Inst. Komp'yut. Issled., 2007)
10. Anishchenko V S *Slozhnye Kolebaniya v Prostykh Sistemakh. Mekhanizmy Vozniknoveniya, Struktura i Svoistva Dinamicheskogo Khaosa v Radiofizicheskih Sistemakh* (Complex Oscillations in Simple Systems. The Mechanisms of Occurrence, Structure and Properties of Chaos in Radiophysical Systems) (Moscow: URSS, 2009)
11. Kuznetsov S P *Dinamicheskii Khaos* (Dynamical Chaos) (Moscow: Fizmatlit, 2006)
12. Strogatz S H *Nonlinear Dynamics and Chaos*: *With Applications to Physics, Biology, Chemistry, and Engineering* (Boulder, CO: Westview Press, 2001)
13. Ott E *Chaos in Dynamical Systems* (Cambridge: Cambridge Univ. Press, 2002)
14. Smale S *Bull. Amer. Math. Soc. New Ser.* **73** 747 (1967)
15. Williams R F *Publ. Math. Inst. Hautes Étud. Sci.* **43** 169 (1974)
16. Sinai Ya G, in *Nelineynye Volny* (Nonlinear Waves) (Ed. A V Gaponov-Grekhov) (Moscow: Nauka, 1979) p. 192
17. *Dinamicheskie Sistemy-9* (Itogi Nauki i Tekhniku. Ser. Sovremennye Problemy Matematiki. Fundamental'nye Napravleniya) (Dynamical Systems-2 (Reviews of Science and Technology. Ser. Modern Problems of Mathematics. Fundamental Directions)) Vol. 66 (Moscow: VINITI, 1991)
18. Eckmann J-P, Ruelle D *Rev. Mod. Phys.* **57** 617 (1985)
19. Shilnikov L *Int. J. Bifurcat. Chaos* **7** 1953 (1997)
20. Katok A, Hasselblatt B *Introduction to the Modern Theory of Dynamical Systems* (Cambridge: Cambridge Univ. Press, 1996) [Translated into Russian (Moscow: Faktorial, 1999)]
21. Guckenheimer J, Holmes P *Nonlinear Oscillations*: *Dynamical Systems, and Bifurcations of Vector Fields* (Berlin: Springer, 1990) [Translated into Russian (Moscow-Izhevsk: Inst. Komp'yut. Issled., 2002)]
22. Afraimovich V, Hsu S-B *Lectures on Chaotic Dynamical Systems* (AMS/IP Studies in Advanced Mathematics, Vol. 28) (Providence, RI: American Mathematical Society, 2003)
23. Hasselblatt B, Katok A A *First Course in Dynamics*: *with a Panorama of Recent Developments* (Cambridge: Cambridge Univ. Press, 2003) [Translated into Russian (Moscow: Izd. MTSNMO, 2005)]
24. Devaney R L *An Introduction to Chaotic Dynamical Systems* (New York: Westview Press, 2003)
25. Anishchenko V S et al. *Nelineinye Effekty v Khaoticheskih i Stokhasticheskikh Sistemakh* (Nonlinear Dynamics of Chaotic and Stochastic Systems) (Moscow-Izhevsk: Inst. Komp'yut. Issled., 2003) [Translated into english (Berlin: Springer, 2007)]
26. Barreira L, Pesin Y, in *Smooth Ergodic Theory and Its Applications* (Proc. of Symp. in Pure Mathematics, Vol. 69) (Providence, RI: American Mathematical Society, 2001) p. 3
27. Bonatti C, Díaz L J, Viana M *Dynamics Beyond Uniform Hyperbolicity. A Global Geometric and Probobalistic Perspective* (Encyclopedia of Mathematical Sciences, Vol. 102. Mathematical Physics 3) (Berlin: Springer, 2005)
28. Benedicks M, Carleson L *Ann. Math.* **133** 73 (1991)
29. Andronov A A, Pontryagin L S *Dokl. Akad. Nauk SSSR* **14** 247 (1937) [*C.R.* (*Dokl.*) *Acad. Sci. USSR* **14** 247 (1937)]
30. Andronov A A, Vitt A A, Khaikin S E *Teoriya Kolebanii* (Theory of Oscillations) (Moscow: Fizmatgiz, 1959) [Translated into English (Oxford: Pergamon Press, 1966)]
31. Benettin G et al. *Meccanica* **15** 9 (1980)
32. Kaplan J L, Yorke J A, in *Functional Differential Equations and Approximation of Fixed Points* (Lecture Notes in Mathematics, Vol. 730, Eds H-O Peitgen, H-O Walther) (Berlin: Springer-Verlag, 1979) p. 204
33. Vul E B, Sinai Ya G, Khanin K M *Usp. Mat. Nauk* **39** (3) 3 (1984) [*Russ. Math. Surv.* **39** 1 (1984)]
34. Coudene Y *Notices Am. Math. Soc.* **53** (1) 8 (2006)
35. Plykin R V *Mat. Sb.* **94** (2) 243 (1974) [*Math. USSR Sb.* **23** (2) 233 (1974)]
36. Zhirov A Yu *Mat. Sb.* **185** (6) 3 (1994) [*Russ. Acad. Sci. Sb. Math.* **82** 135 (1995)
37. Grines V Z, Zhuzhoma E V *Regul. Chaotic Dyn.* **11** (2) 225 (2006)
38. Feller W *An Introduction to Probability Theory and Its Applications* Vol. 1 (New York: Wiley, 1968) [Translated into Russian (Moscow: Mir, 1984)]
39. Adler R L, Konheim A G, McAndrew M H *Trans. Am. Math. Soc.* **114** 309 (1965)
40. Beck C, Schlögl F *Thermodynamics of Chaotic Systems*: *An Introduction* (Cambridge: Cambridge Univ. Press, 1993)
41. Kifer Ju I *Izv. Akad. Nauk SSSR. Ser. Mat.* **38** 1091 (1974) [*Math. USSR Izv.* **8** 1083 (1974)
42. Sinai Ya G *Usp. Mat. Nauk* **27** (4) 21 (1972) [*Russ. Math. Surv.* **27** (4) 21 (1972)
43. Bowen R *Equilibrium States and the Ergodic Theory of Anosov Diffeomorphisms* (Lecture Notes in Math., Vol. 470) (Berlin: Springer-Verlag, 1975)
44. Ruelle D *Am. J. Math.* **98** 619 (1976)
45. Kolmogorov A N *Dokl. Akad. Nauk SSSR* **124** 754 (1959)
46. Sinai Ya G *Dokl. Akad. Nauk SSSR* **124** 768 (1959)
47. Pesin Ya B *Usp. Mat. Nauk* **32** (4) 55 (1977) [*Russ. Math. Surv.* **32** (4) 55 (1977)]
48. Ruelle D, Takens F *Commun. Math. Phys.* **20** 167 (1971) [Translated into Russian, in *Strannye Attraktory* (Eds Ya G Sinai, L P Shil'nikov) (Moscow: Mir, 1981) p. 117]
49. Newhouse S, Ruelle D, Takens F *Commun. Math. Phys.* **64** 35 (1978)
50. Lorentz E N *J. Atmos. Sci.* **20** 130 (1963) [translated into Russian , in *Strannye Attraktory* (Eds Ya G Sinai, L P Shil'nikov) (Moscow: Mir, 1981) p. 88]
51. Tucker W *Found. Comput. Math.* **2** 53 (2002)
52. Morales C A *Ann. Inst. Henri Poincaré Non Linéaire* **13** 589 (1996)
53. Lopes A O, in *Geometric Dynamics* (Lecture Notes in Mathematics, Vol. 1007, Ed. J Palis) (Berlin: Springer-Verlag, 1983) p. 498
54. Hunt T J "Low dimensional dynamics: bifurcations of cantori and realisations of uniform hyperbolicity", PhD Thesis (Cambridge: Univ. of Cambridge, 2000)
55. Akhiezer N I *Elementy Teorii Ellipticheskikh Funktsii* (Elements of the Theory of Elliptic Functions) (Moscow: Nauka, 1970) [Translated into English (Providence, RI: Am. Math. Soc., 1999)]
56. Aidarova Yu S, Kuznetsov S P *Izv. Vyssh. Ucheb. Zaved. Priklad. Nelin. Dinamika* **16** (3) 176 (2008); arXiv:0901.2727
57. Hunt T J , MacKay R S *Nonlinearity* **16** 1499 (2003)
58. Thurston W P, Weeks J R *Sci. Am.* **251** (1) 94 (1984) [*V Mire Nauki* (9) 74 (1984)
59. Belykh V, Belykh I, Mosekilde E *Int. J. Bifurcat. Chaos* **15** 3567 (2005)
60. González-Miranda J M *Int. J. Bifurcat. Chaos* **17** 3071 (2007)
61. Turaev D V, Shil'nikov L P *Dokl. Ross. Akad. Nauk* **342** 596 (1995) [*Dokl. Math.* **51** 404 (1995)]
62. Shil'nikov L P, Turaev D V *Comput. Math. Appl.* **34** (2 – 4) 173 (1997)
63. Gavrilov N K, Shilnikov A L *Am. Math. Soc. Transl. II* **200** 165 (1999)
64. Shilnikov A, Cymbalyuk G *Phys. Rev. Lett.* **94** 048101 (2005)
65. Glyzin S D, Kolesov A Yu, Rozov N Kh *Differ. Equat.* **44** (2) 161 (2008)
66. Kuznetsov S P *Regul. Chaotic Dyn.* **15** (2–3) 348 (2010)
67. Halbert J T , Yorke J A, http://www.math.umd.edu/~halbert/taffy-paper-1.pdf
68. Reichl L E *The Transition to Chaos*: *Conservative Classical Systems and Quantum Manifestations* (New York: Springer, 2004)
69. Heagy J F *Physica D* **57** 436 (1992)
70. Kuznetsov A P, Savin A V, Savin D V *Physica A* **387** 1464 (2008)
71. Tyuryukina L V *Nelineinyi Mir* **8** (2) 72 (2010)
72. Kuznetsov S P, Tyuryukina L V *Izv. Vyssh. Ucheb. Zaved. Priklad. Nelin. Dinamika* **18** (5) 80 (2010)
73. Kuznetsov S P *Commun. Nonlinear Sci. Numerical Simulation* **14** 3487 (2009)

74. Kuznetsov S P *Nelin. Dinamika* **5** (3) 403 (2009)
75. Kuznetsov S P *Chaos* **19** 013114 (2009)
76. Klyshko D N *Fizicheskie Osnovy Kvantovoi Elektroniki* (Physical Principles of Quantum Electronics) (Moscow: Nauka, 1986)
77. Rozenberg G V *Usp. Fiz. Nauk* **56** 77 (1955)
78. Kuznetsov S P *Phys. Rev. Lett.* **95** 144101 (2005)
79. Isaeva O B, Jalnine A Yu, Kuznetsov S P *Phys. Rev. E* **74** 046207 (2006)
80. Isaeva O B, Kuznetsov S P, Osbaldestin A *Pis'ma Zh. Teor. Fiz.* **33** (17) 69 (2007) [*Tech. Phys. Lett.* **33** 748 (2007)]
81. Isaeva O B, Kuznetsov S P, Osbaldestin A H *Physica D* **237** 873 (2008)
82. Zhalnin A Yu, Kuznetsov S P *Zh. Tekh. Fiz.* **77** (4) 10 (2007) [*Tech. Phys.* **52** 401 (2007)
83. Kuptsov P V, Kuznetsov S P *Nelin. Dinamika* **2** (3) 307 (2006)
84. Kuznetsov S P, Sataev I R *Izv. Vyssh. Ucheb. Zaved. Priklad. Nelin. Dinamika* **14** (5) 3 (2006)
85. Kuznetsov S P, Sataev I R *Phys. Lett. A* **365** 97 (2007)
86. Wilczak D *SIAM J. Appl. Dyn. Sys.* **9** 1263 (2010)
87. Kuptsov P V, Kuznetsov S P, Sataev I R, arXiv: 0804.3677
88. Kuznetsov A P, Kuznetsov S P, Pikovskii A S, Tyuryukina L V *Izv. Vyssh. Ucheb. Zaved. Priklad. Nelin. Dinamika* **15** (6) 75 (2007)
89. Kuznetsov S P, Pikovsky A *Physica D* **232** 87 (2007)
90. Kuznetsov S P, Pikovsky A, Sataev I R, in *Proc. of the III Intern. Conf. "Frontiers of Nonlinear Physics"* (Nizhny Novgorod: IAP RAS, 2007) p. 66
91. Louisell W H *Coupled Mode and Paramagnetic Electronics* (New York: Wiley, 1960) [Translated into Russian (Moscow: IL, 1963)]
92. Akhmanov S A, Khokhlov R V *Usp. Fiz. Nauk* **88** 439 (1966) [*Sov. Phys. Usp.* **9** 210 (1966)]
93. Kuznetsov A P, Kuznetsov S P, Ryskin N M *Nelineynye Kolebaniya* (Nonlinear Oscillations) (Moscow: Fizmatlit, 2005)
94. Kuznetsov S P *Zh. Eksp. Teor. Fiz.* **133** 438 (2008) [*JETP* **106** 380 (2008)]
95. Kuznetsov A S, Kuznetsov S P, Sataev I R *Zh. Tekh. Fiz.* **80** (12) 1 (2010) [*Tech. Phys.* **55** 1707 (2010)]
96. Kuznetsov S P, Ponomarenko V I *Pis'ma Zh. Tekh. Fiz.* **34** (18) 1 (2008) [*Tech. Phys. Lett.* **34** 771 (2008)]
97. Kuznetsov S P, Pikovsky A *Europhys. Lett.* **84** 10013 (2008)
98. Baranov S V, Kuznetsov S P, Ponomaremko V I *Izv. Vyssh. Ucheb. Zaved. Priklad. Nelin. Dinamika* **18** (1) 11 (2010)
99. Kuznetsov S P, Seleznev E P *Zh. Eksp. Teor. Fiz.* **129** 400 (2006) [*JETP* **102** 355 (2006)]
100. Emel'yanov V V, Kuznetsov S P, Ryskin N M *Pis'ma Zh. Tekh. Fiz.* **35** (16) 71 (2009) [*Tech. Phys. Lett.* **35** 773 (2009)]
101. Wolf A et al. *Physica D* **16** 285 (1985)
102. Bunimovich L A, Sinai Ya G *Nonlinearity* **1** 491 (1988)
103. Bunimovich L A, Sinai Ya G, in *Theory and Application of Coupled Map Lattices* (Ed. K Kaneko) (Singapore: John Wiley, 1993) p. 169
104. Kuptsov P V, Kuznetsov S P *Phys. Rev. E* **80** 016205 (2009)
105. Dmitriev A S, Panas A I *Dinamicheskii Khaos: Novye Nositeli Informatsii dlya Sistem Svyazi* (Dynamical Chaos: New Information Carriers for Communication Systems) (Moscow: Fizmatlit, 2002)
106. Yang T *Int. J. Comput. Cognition* **2** (2) 81 (2004)
107. Argyris A et al. *Nature* **438** 343 (2005)
108. Koronovskii A A, Moskalenko O I, Hramov A E *Usp. Fiz. Nauk* **179** 1281 (2009)[*Phys. Usp.* **52** 1213 (2009)]
109. Banerjee S, Yorke J A, Grebogi C *Phys. Rev. Lett.* **80** 3049 (1998)
110. Elhadj Z, Sprott J C *Front. Phys. China* **3** (2) 195 (2008)
111. Drutarovský M, Galajda P *Radioengineering* **16** (3) 120 (2007)